Nano-Scale Imaging Using Coherent Hard X-rays
VH-VI-203

Virtuelles Instituts im Rahmen des Impuls- und
Vernetzungsfonds des Präsidenten der Helmholtz-Gemeinschaft

Abschlussbericht
(Sachlicher Teil)
15.03.2011

An die Geschäftsstelle der Helmholtz-Gemeinschaft
Ahrstraße 45 53175 Bonn

1. Allgemeines / General Information

Leitende Wissenschaftler der beteiligten Gruppen:

Georg-August-University Göttingen Institut für Röntgenphysik
Prof. Dr. Tim Salditt (Sprecher)
Friedrich-Hund-Platz 1
D-37077 Göttingen
e-mail: tsaldit@gwdg.de
Tel.: 0551 399427
Fax: 0551 399430

Technische Universität Dresden
Institut für Strukturphysik
Prof. Dr. Christian Schroer
Zellescher Weg 16
D-01062 Dresden
e-mail: schroer@physik.tu-dresden.de
Tel.: 0351 463 37589
Fax: 0351 463 37048

Deutsches Elektronensynchrotron
Hamburger Synchrotronstrahlungslabor
Dr. Ivan Vartaniants
Notkestr. 85
D-22607 Hamburg
email: ivan.vartaniants@desy.de
Tel.: 040 8998 2653
Fax: 040 8998 4475

Federführendes Helmholtz-Zentrum:

Deutsches Elektronensynchrotron
Hamburger Sychrotronstrahlungslabor
Prof. Dr. Edgar Weckert
Notkestr. 85
D-22607 Hamburg
e-mail: edgar.weckert@desy.de
Tel.: 040 8998 4509
Fax: 040 8998 4475

1.1 List of Publications

Publications with partial VI support and publications of the participating groups related to the subject of the VI (peer reviewed, original publications)

2008

T. Salditt, S. P. Krüger, C. Fuhse, C. Bahtz
"High-transmission planar x-ray waveguides"
Phys. Rev. Lett. **100**, 184801 (2008)

B. Enders, K. Giewekemeyer, T. Kurz, S. Podorov and T. Salditt
"*Non-iterative coherent diffractive imaging using a phase-shifting reference frame"*
New J. Phys. **11** (2009) 043021

A.V. Zozulya, O. M. Yefanov, I.A. Vartanyants, K. Mundboth, C. Mocuta, T.H. Metzger, J. Stangl, G. Bauer, T. Boeck, and M. Schmidbauer,
"Imaging of nanoislands in coherent grazing-incidence small-angle x-ray scattering experiments",
Phys. Rev. B Rapid Communications **78**, 121304(R)/1-4 (2008).

A. Singer, I.A. Vartanyants, M. Kuhlmann, S. Duesterer, R. Treusch, and J. Feldhaus
"Transverse-Coherence Properties of the Free-Electron-Laser FLASH at DESY"
Phys. Rev. Lett. **101**, 254801 (2008).

C. G. Schroer, P. Boye, J. Feldkamp, J. Patommel, A. Schropp, A. Schwab, S. Stephan, M. Burghammer, S. Schöder, C. Riekel, "*Coherent x-ray diffraction imaging with nanofocused illumination"*, Phys. Rev. Lett **101**, 090801 (2008).

M. Hanke, M. Dubslaff, M. Schmidbauer, T. Boeck, S. Schöder, M. Burghammer, C. Riekel, J. Patommel, C. G. Schroer, "*Scanning x-ray diffraction with 200 nm spatial resolution"*, Appl. Phys. Lett. **92**, 193109 (2008).

E. Nováková, G. Mitrea, C. Peth, J. Thieme, K. Mann, T. Salditt "*Solid supported multicomponent lipid membranes studied by x-ray spectromicroscopy"* Biointerphases Volume 3, Issue 2, FB44-FB45 (2008)

T. Hohage, K. Giewekemeyer, T. Salditt "*Iterative reconstruction of a refractive-index profile from x-ray or neutron reflectivity measurements"* Physical review E, 77(5), 051604 (2008

A. Kohlstedt, S. Kalbfleisch, T. Salditt, M. Reiche, U. Gösele, E. Lima, P. Willmott
"*Two-dimensional X-ray waveguides: fabrication by wafer-bonding process and characterization"*,
Applied Physics A 91, 6-12 (2008)

S. Panknin , A. K. Hartmann, T. Salditt
"X-Ray Propagation in Tapered Waveguides: Simulation and Optimization"
Optics Communication, in press

2009

A.P. Mancuso, A. Schropp, B. Reime, L.-M. Stadler, A. Singer, J. Gulden, S. Streit-Nierobisch, C. Gutt, G. Grübel, J. Feldhaus, F. Staier, R. Barth, A. Rosenhahn, M. Grunze, T. Nisius, T. Wilhein, D. Stickler, H. Stillrich, R. Frömter, H.P. Oepen, M. Martins, B. Pfau, C.M. Günther, R. Könnecke, S. Eisebitt, B. Faatz, N. Guerassimova, K. Honkavaara, V. Kocharyan, R. Treusch, E. Saldin, S. Schreiber, E.A. Schneidmiller, M.V. Yurkov, E. Weckert, and I.A. Vartanyants
"Coherent-pulse 2D Crystallography at Free Electron Lasers"
Phys. Rev. Lett. **102**, 035502/1-5 (2009).

O. M. Yefanov, and I.A. Vartanyants,
"Three dimensional reconstruction of nanoislands from grazing-incidence small-angle X-ray scattering"
The European Physical Journal Special Topics **167**, 81-86 (2009).

O. M. Yefanov, A.V. Zozulya, I.A. Vartanyants, J. Stangl, C. Mocuta, T.H. Metzger, G. Bauer, T. Boeck, and M. Schmidbauer,
"Coherent diffraction tomography of nanoislands from grazing-incidence small-angle x-ray scattering"
Appl. Phys. Lett. **94**, 123104 (2009).

A. Rosenhahn, F. Staier, Th. Nisius, D. Schäfer, R. Barth, C. Christophis, L.-M. Stadler, S. Streit-Nierobisch, C. Gutt, A. Mancuso, A. Schropp, J. Gulden, B. Reime, J. Feldhaus, E. Weckert, B. Pfau, C. M. Günther, R. Könnecke., S. Eisebitt, M. Martins, B. Faatz, N. Guerassimova, K. Honkavaara, R. Treusch, E. Saldin, S. Schreiber, E. A. Schneidmiller, M. V. Yurkov, I. Vartaniants, G. Grübel, M. Grunze, Th. Wilhein "Digital In-line Holography with femtosecond VUV radiation provided by the Free-electron laser FLASH" Optics Express **17,** No. 10, 8220-8228 (2009).

T. Salditt, K. Giewekemeyer, C. Fuhse, S. P. Krüger, R. Tucoulou, P. Cloetens "*Projection phase contrast microscopy with a hard x-ray nanofocused beam: Defocus and contrast transfer"* Phys. Rev. B 79, 184112 (2009)

B. Enders, K. Giewekemeyer, T. Kurz, S. Podorov, T. Salditt "*Non-iterative coherent diffractive imaging using a phase-shifting reference frame"* New J. Phys. 11, 043021 (2009)

A. Beerlink, M. Mell, M. Tolkiehn, T. Salditt "*Hard x-ray phase contrast imaging of black lipid membranes"* Applied Physics Letters 95, 203703 (2009)

2010

K. Giewekemeyer, S. P. Krüger, S. Kalbfleisch, M. Bartels, C. Beta, T. Salditt "*X-ray propagation microscopy of biological cells using waveguides as a quasipoint source*"Phys. Rev. A 83, 023804 (2011)

S. P. Krüger, K. Giewekemeyer, S. Kalbfleisch, M. Bartels, H. Neubauer, T. Salditt "*Sub-15 nm beam confinement by two crossed x-ray waveguides"* Opt. Express 18, 13492-13501 (2010)

K. Giewekemeyer, P. Thibault, S. Kalbfleisch, A. Beerlink, C. M. Kewish, M. Dierolf, F. Pfeiffer and T. Salditt "*Quantitative biological imaging by ptychographic x-ray diffraction microscopy* " PNAS January 12, vol. 107 no. 2 529-534 (2010)

K. Giewekemeyer, H. Neubauer, S. Kalbfleisch, S. P. Krüger and T. Salditt "*Holographic and diffractive and x-ray imaging using waveguides as quasi-point sources"* New Journal of Physics 12 (2010)

C. Gutt, S. Streit-Nierobisch, L.-M. Stadler, B. Pfau, C.M. Guenther,R. Koennecke, R. Froemter, A. Kobs, D. Stickler, H. P. Oepen, R.R. Faeustlin, R. Treusch, J. Feldhaus, E. Weckert, I. A. Vartanyants, M. Grunze, A. Rosenhahn, T. Wilhein, S. Eisebitt, and G. Gruebel,
"*Single-pulse resonant magnetic scattering using a soft x-ray free-electron laser*",
Phys. Rev. B 81, 100401(R) (Rapid Commun.), (2010).

A. Mancuso and I. A. Vartanyants
"Coherent-Pulse 2D Crystallography at Free-Electron Lasers. Towards higher resolution from the world's brightest sources"
Photon Science 2009. Highlights and HASYLAB Annual Report, p. 34-35 (2010).

C. G. Schroer, P. Boye, J. M. Feldkamp, J. Patommel, A. Schropp, D. Samberg, S. Stephan, M. Burghammer, S. Schöder, C. Riekel, B. Lengeler, G. Falkenberg, G. Wellenreuther, M. Kuhlmann, R. Frahm, D. Lützenkirchen-Hecht, and W. H. Schroeder
"Hard X-ray microscopy with elemental, chemical, and structural contrast", Acta Physica Polonica A 117, 357 (2010).
A. Schropp, P. Boye, J. M. Feldkamp, R. Hoppe, J. Patommel, D. Samberg, S. Stephan, K. Giewekemeyer, R. N. Wilke, T. Salditt, J. Gulden, A. P. Mancuso,I. A. Vartanyants, E. Weckert, S. Schoeder, M. Burghammer, and C. G. Schroer
"Hard x-ray nanobeam characterization by coherent diffraction microscopy", Appl. Phys. Lett. 96, 091102 (2010).

C. G. Schroer, P. Boye, J. M. Feldkamp, J. Patommel, D. Samberg, A. Schropp, A. Schwab, S. Stephan, G. Falkenberg, G. Wellenreuther, and N. Reimers
"Hard X-ray nanoprobe at beamline P06 at PETRA III", Nucl. Instrum. Meth. A 616(2-3), 93 (2010).

A. Schropp and C. G. Schroer
"Dose requirements for resolving a given feature in an object by coherent x-ray diffraction imaging". New Journal of Physics, 12, 035016 (2010).
A.P. Mancuso, O.M. Yefanov, and I. A. Vartanyants
"*Coherent Diffractive Imaging of Biological Samples at Synchrotron and Free Electron Laser Facilities* ",
Journal of Biotechnology, (2010). Published Online: 16-MAR-2010. DOI: 10.1016/j.jbiotec.2010.01.024.

A.P. Mancuso, Th. Gorniak, F. Staier, O.M. Yefanov, R. Barth, C. Christophis, B. Reime, J. Gulden, A. Singer, M.E. Pettit, Th. Nisius, Th. Wilhein, C. Gutt, G. Grübel, N. Guerassimova, R. Treusch, J. Feldhaus, S. Eisebitt, E. Weckert, M. Grunze, A. Rosenhahn and I. A. Vartanyants
"Coherent imaging of biological samples with femtosecond pulses at the free-electron laser FLASH",
Focus issue: Focus on X-ray beams with high coherence. New J. Phys. 12 035003 (2010)
I.A. Vartanyants, A. Singer,

"Coherence Properties of Hard X-Ray Synchrotron Sources and X-Ray Free-Electron Lasers", Focus issue: Focus on X-ray beams with high coherence. New J. Phys. 12 035004 (2010)

J. Gulden, O.M. Yefanov, A.P. Mancuso, V.V. Abramova, J. Hilhorst, D. Byelov, I. Snigireva, A. Snigirev, A.V. Petukhov, and I.A. Vartanyants
" Coherent x-ray imaging of defects in colloidal crystals", Phys. Rev. B Vol. 81, No. 22, 224105 (2010), DOI: 10.1103/PhysRevB.81.224105.

I. A. Vartanyants, A. P. Mancuso, A. Singer, O.M. Yefanov, and J. Gulden,
Coherence Measurements and Coherent Diffractive Imaging at FLASH", Special issue: Intense x-ray science: The first 5 years of FLASH", J. Phys. B: At. Mol. Opt. Phys. 43, 194016 (2010), published on-line: http://stacks.iop.org/0953-4075/43/194016.

M. Altarelli, R. Kurta, and I. A. Vartanyants
" X-ray cross-correlation analysis and local symmetries of disordered systems: General theory ", Phys. Rev. B 82, No.10, 104207 (2010)

2011

A. Schropp, P. Boye, A. Goldschmidt, S. Hönig, R. Hoppe, J. Patommel, C. Rakete, D. Samberg, S. Stephan, S. Schöder, M. Burghammer, and C. G. Schroer
"*Non-destructive and quantitative imaging of a nano-structured microchip by ptychographic hard x-ray scanning microscopy"*. J. Microscopy, 241(1), 9 (2011).

K. Giewekemeyer, S.P. Krüger, S. Kalbfleisch, M. Bartels, C. Beta, and T. Salditt
„X-ray propagation microscopy of biological cells using waveguides as a quasipoint source."
Phys. Rev. A 023804 (2011)

In the first year after ending of the project, not all of the research results are fully evaluated yet. In particular joint beamtimes at FLASH have been carried out in 2010. As a matter of course, the data/ results are not published yet, but are still being analyzed. Other results of coherent x-ray imaging are written up, or have been submitted, but are not listed here.

1. 2 Qualifications obtained within the project / support of young investigators

The support of the VI has been instrumental in the support of young scientists entering the research field and making significant contributions. Without claim of completeness, the Ph.D. thesis work of the following young investigators has been enabled or supported by the VI.

Ph.D. completed: K. Giewekemeyer, S. Krüger (U Gö), P. Boye (TU Dresden), J. Feldkamp (TU Dresden), J. Patommel (TU Dresden)

Ph.D. (ongoing): S. Kalbfleisch (U Gö), H. Neubauer (U Gö), M. Osterhoff (U Gö), S. Stephan (TU Dresden), J. Gulden (DESY), A. Singer (DESY)

Postdoctoral research: A. Schropp (TU Dresden), O.M. Yefanov (DESY), M. Tolkiehn (U Gö)

The VI has also increased the awareness of the young investigators, in particular in the university groups, that the Helmholtz center offers attractive career opportunities in the research field. Several group members have accepted attractive job offers at HASYLAB/DESY. From Göttingen University alone, three group members (Dr. Tanja Ducic, Dr. Andre Beerlink, Dr. Martin Tolkiehn) have joint HASYLAB/DESY, after completing their research at the University. Dr. J. Feldkamp (formerly TU Dresden) joint the LCLS as a postdoctoral fellow. This has led to a very fruitful network between the institutions, facilitating collaborations and transfer of know-how.

1.3 Joint meetings and workshops

About (on average) two VI meetings per year have been held to coordinate and discuss the joint research. In particular common beamtimes and public conferences /workshops have provided additional occasions for coordination/discussion.

The following VI meetings have been held:

7.7.2007 Göttingen: Opening Workshop
"Imaging at nano-scale samples with coherent x-rays"
Talks and Discussion, procedures
Discussion on aspects of the coherence beamline at PETRA III

19.10.2007 Dresden
Talks. discussion, preparation of common beamtime

7.3.2008 Hamburg
Talks, Discussion, in particular on data analysis

15.4.2008 TU Dresden: meeting T. Salditt, C. Schroer, discussion on VI related research activities, talk

11.9.2009 HASYLAB/DESY: talks and discussion, preparation of beamtimes

Several public workshops related to the VI research topic have been organized by VI principal investigators, and have provided additional opportunities for VI members to interact

Research Course on New X-ray Sciences "New Materials in New Light" March 5-7, 2008 at DESY, Hamburg
Organizers: I. Vartaniants, R. Feidenhans'l, Th. Tschentscher

404 WE-Heraeus-Seminar "Matter in Coherent Light", March 17-20, 2008 at the Physikzentrum Bad Honnef, Germany. Organizers: E. Weckert, G. Gruebel, I. Vartaniants

Talks related to VI project:

Christian Schroer

29.10.2010	Seminar, KIT, Karlsruhe *Hard X-Ray Microscopy with Elemental, Chemical, and Structural Contrast*
17.08.2010	XRM 2010, Chicago, USA *Hard X-Ray Microscopy with Coherent Diffraction Contrast*
08.04.2010	IFW Seminar, Dresden *Hard X-Ray Microscopy and Nanoanalysis*
25.02.2010	SNI 2010, Berlin (plenary, invited) Rastermikroskopie und -tomographie mit harter Röntgenstrahlung
09.02.2010	Workshop ”Science with X-Ray Nanobeams,“ ESRF, France (invited) *Hard X-Ray Microscopy with Coherent Diffraction Contrast*
29.01.2010	HASYLAB Usermeeting, DESY, Hamburg (invited) *Mapping the local structure of thin films by GISAXS-tomography*
12.01.2010	Graduiertenkolleg ”Physics with new advanced coherent radiation sources“, Universität Hamburg *Microscopy with Coherent Hard X Rays*
08.10.2009	Institutsseminar des IIM, FZD Rossendorf *Microscopy and Tomography Using Hard X-Rays*
22.09.2009	International Workshop on X-Ray Mirrors and Metrology, Osaka, Japan (invited) *Hard X-Ray Scanning Microscope Based on Refractive X-Ray Lenses*
15.05.2009	CXDI Consortium Meeting, HASYLAB, Hamburg *CXDI with Nanofocused Illumination at XFEL*
06.03.2009	Workshop of the Coherence BL P10, DESY (invited) *Coherent Imaging with Nanofocused Beams*
25.02.2009	SMEXOS, ESRF (invited) *Wave-Optical Modeling of Hard X-Ray Transmission Optics*
16.01.2009	Seminar, GFZ Potsdam *X-Ray Microscopy and Tomography in Fluorescence, Absorption, and Diffraction Contrast*
07.10.2008	XAS08, PSI Villigen, Schweiz (invited) *XAS Microscopy and Tomography*

18.09.2008	XTOP 2008, Linz, Östereich *Coherent X-ray Diffraction Imaging with Nanofocused Illumination*
07.08.2008	Workshop on Time-Resolved X-Ray Analysis, MPI-PKS, Dresden (invited) *Coherent Diffraction Imaging with a Hard X-Ray Nanobeam*
22.07.2008	XRM2008, Zürich, Schweiz Hard X-Ray Scanning Microscopy with Fluorescence and Diffraction Contrast
18.07.2008	Diamond Light Source, Didcot, UK *Hard X-Ray Nanoprobe Based on Refractive X-Ray Lenses*
09.07.2008	BMBF Verbundforschungstreffen bei DESY, Hamburg Hard X-Ray Scanning Microscopy with Fluorescence and Diffraction Contrast
18.03.08	404. Heraeusseminar Matter in Coherent Light, Bad Honnef Wave-Optical Properties of Refractive X-Ray Lenses (invited)
07.03.08	VI-203 Meeting at DESY Nano-Coherent X-Ray Diffraction Imaging
15.11.07	Prozessnahe Röntgenanalytik ProRA2007, Berlin Refraktive Optiken für die Röntgenmikroskopie
24.10.07	ESRF Upgrade Meeting, Grenoble (invited) PETRA III: Hard X-ray Micro- and Nanoprobe
17.07.07	Festkörperanalytik, Wien (keynote lecture) Mikroskopie und Tomographie mit analytischem Kontrast
04.07.07	1st Meeting of the Virtual Institute VI-203 in Göttingen Coherent Diffraction Imaging with Small Beams
23.04.07	Upgrade Workshop, Argonne, IL, USA (invited) Nanofocusing Hard X Rays with Refractive Lenses

Ivan Vartaniants

15.01.08	Physics-Colloquium Technical University, Dresden Coherent X-ray Diffraction of Nanometer Size Object
19.02.08	Workshop on Photon Science with Applications to Nano- and Life- Science, RRC “Kurchatov Intitute”, Moscow, Russia Coherent X-ray Scattering at Synchrotron and FEL Sources
23.01.08	Physics-Colloquium, Bohr Institute, University of Copenhagen, Copenhagen

	Coherent Diffractive Imaging at Synchrotron and FEL Sources
07.03.08	Physics-Colloquium, Rostock University Coherent X-ray Diffractive Imaging of Nanometer Size Crystals

Tim Salditt

06.01.11	Physics Colloquium, University of Bremen X-Ray vision at the nanoscale: imaging of membranes and cells
20.01.11	Physics Colloquium, University of Berlin X-ray holographic imaging of cells and membranes
15./16.11.10	Molecules under X-ray pulses 10: International Focus Workshop (MolX 10), Dresden Biological Imaging: from synchrotron to FEL
28.07.10	Stanford, Linac Coherent Light Source (LCLS) "Coherent x-ray imaging of biological cells and membranes: data recording and phase reconstruction in the holographic setting"
Aug. 2010	Kavli Institute for Theoretical Physics, Santa Barbara KITP Program Frontiers in X-ray Science in the 21st Century
25.07.10	University of California, Los Angeles (inv. Prof. Dr. John Miao) Physics Seminar
27.07.10	Advanced Light Source, Berkeley, (inv. Prof Janos Kirz) Seminar Talk
11.02.10	Workshop "Science with X-ray Nano-beams", ESRF, Grenoble X-ray imaging with nanoscale beams: phase contrast fluorescence and diffraction"
15.01.10	Colloquium of the Inst. for Atomic and Optical Physics, University of Jena Lensless coherent x-ray imaging of cells
15.08.–19.08.09	European Crystallographic Meeting 25 (ECM 25), Istanbul Microsymposium: Coherent x-ray diffraction and imaging in biology (Chair & Organizer)
26.08.09	bioImaging 4. CeBiTec Symposium 2009, Zentrum für innovative Forschung Bielefeld Biological imaging with coherent lensless x-ray microscopy
05.03.09	PETRA III workshop P10 Coherent x-ray imaging of Biological Cells and Biomaterials

25.02.-27.02.09	Neutrons and x-rays meet biology workshop Helmholtz-Zentrum, Berlin Structure and dynamics of lipid membranes: from scattering to Imaging
29.01.09	XFEL Consortium Meeting Hamburg Diffraction from biomolecular assemblies aligned in a microfluidic jet
15.01.09	Physical Colloquium University of Siegen X-ray imaging as a new tool for biophysics and nanoscience
21.-25.07.08	9th International Conference on x-ray Microscopy, PSI Villigen X-ray imaging with nanoscale beams: phase contrast, fluorescence and diffraction
09.-11.07.08	BMBF Verbundforschungstreffen FLASH und PETRA III New perspectives for coherent x-ray experiments at PETRA III
26.06.08	Microscience 2008, Royal Microscopy Society, Oxford Lense-less x-ray imaging based on holographic object reconstruction
15.04.08	Physics Colloquium, University Dresden Struktur und Dynamik in biologischen Modellmembranen: Von Streuexperimenten zu Abbildungen mit Röntgenstrahlung
07.03.08	Research Course DESY, Hamburg Imaging applications to bio-materials
3.01.08	Nanoprobe@petra3 Workshop, DESY, Hamburg Hard x-ray nanoprobe of biological systems: fluorescence, diffraction and phase contrast
22.01.08	Physics Colloquium, University of Kiel Mit Röntgenaugen im Nanokosmos
14.01.08	Physics Colloquium, University of Erlangen Physik und Anwendungen von Röntgenwellenleitern

2. Research Activities and Results

The research of the VI *Nano-Scale Imaging Using Coherent Hard X-rays* (VH-VI-203) has been reported on an annual basis, including the last year. Therefore, for this final report we have combined the (partial) reports, given previously, with slight editing and shortening.

2.1 Research Activities in 4/2007-4/2008

A coherent diffraction experiment at the newly commissioned cSAXS beamline of PSI was carried out with joint staff from all three groups. The experiments were prepared, carried out, and the data was analyzed in a highly synergistic manner. Special emphasis during the first year of the VI was given to the education and training of PhD and Diploma students in all three groups. The main joint beamtime was carried out with 5 PhD students and 2 Diploma students, mainly in order to disseminate the corresponding knowledge.

Experimental Report on first joint experiment: SLS Proposal ID 20070205

Abstract and Scope - We report on a Coherent Diffraction Imaging (CDI) Experiment at the cSAXS beamline of the SLS. The following goals of the experiment were reached: (A) Instrumentation for CDI methods was tested and benchmarked (pinhole fabrication for illumination, holders and manipulation of biological samples); (B) coherent diffraction data was collected in different modes (slit illumination, pinhole illumination, ptychography) from prefabricated test patterns; (C) CDI was applied to freeze-dried biological cells. To this end, samples of the slime mould *Dictyostelium Discoideum* (Dicty cells) in the vegetative state were measured. While it has been applied to freeze-dried cells using soft x-rays before, the present work is a first-time application of CDI to biological cells in the hard x-ray regime, in particular using the ptychography approach. Work packages and goals (A) and (B) were carried out in the framework of the virtual institute (VI) for coherent x-ray diffraction.

Test samples: (i) Patterns defined in Au on thin (about 150nm Si) foils were fabricated by e-beam lithography followed by lift-off techniques. (ii) Test patterns etched in a 40-80 nm layer of Au deposited on thin Si foils were structured by a focused Ga ion beam (FIB). Both type of samples were used as test objects, with sample cross sections ranging in between 5 μm and 10 μm. The patterns comprised a Siemens star, different logos and resolution objects, including a framed pattern suitable for reconstruction by direct inversion according to the recent algorithm of direct inversion (Podorov, S.G. *et al.* Optics Express 15, 9954, 2007). For illumination, commercial electron microscopy pinholes in 200 μm thick Pt-Ir foils have been used after further treatment of edges by FIB. The test patterns were aligned optically (x-ray scintillator foil).

Biological Samples: Freeze dried Dicty cells attached to polyimide foils (Mitegen, USA) were shock frozen by plunging in liquid ethane. The polyimide foils were fixed on magnetic sample holders (Hampton Research, USA). The position of the sample in the pinhole beam was controlled in-line by phase contrast x-ray imaging (using the scintillator foil with a drilled hole at the cSAXS beamline).

Experimental settings: A photon energy of 6.8 keV (5^{th} undulator harmonic) was set by the Si (111) double monochromator positioned upstream from the (unbent) mirror (SiO_2, 0.2° incidence angle) used for rejection of higher harmonics. Data were taken with a CCD (PI-SCX-4300) with a 1:1 imaging glass fiber system and a high resolution scintillator foil (YAG:Cr). Samples were measured in full beam and ptychography mode. Using the pinhole illumination, the scintillator CCD camera allowed 0.01 sec illumination without using a beamstop. This allowed us to obtain intensity values for the central pixels, which are else hidden by the beamstop (BS). For long exposures, two BS sizes were used (3.5 and 1.5 mm diameters, respectively), and later combined to one image (dynamic synthesis for high dynamic range).

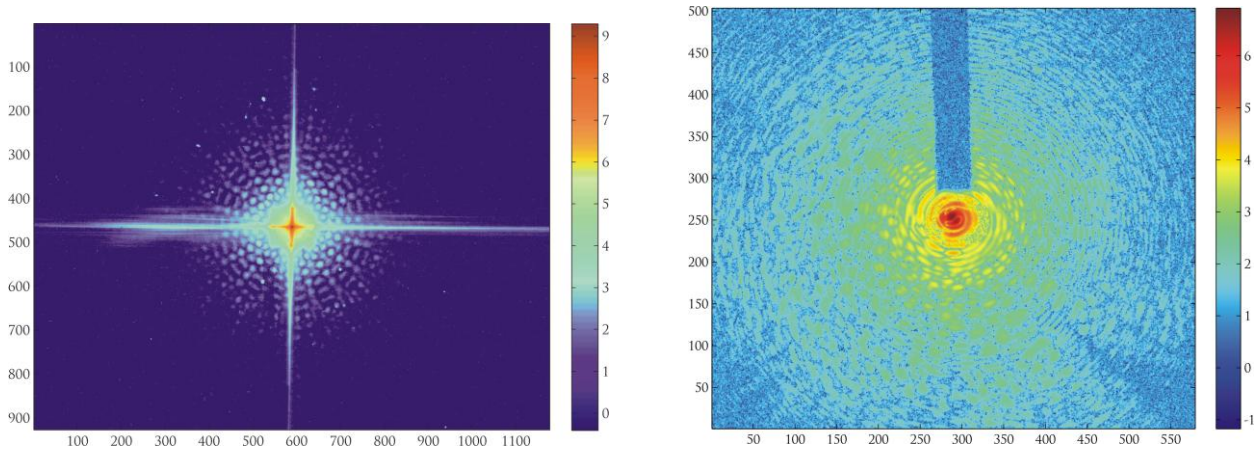

Figure 1: *Farfield pattern of the same siemens star test object ("Fib2_Star"), under two entirely different illumination conditions: (left) Illumination with slit collimation. The farfield is readily identified as that of a siemens star in contrast to (right) , where interference terms between pinhole and object complicate the direct visual interpretation. Note that in (right) the object was positioned behind a 10 µm pinhole (pin#9). A 100 s exposure with beamstop has been merged with a short exposure without beamstop to illuminate the central part (dynamic synthesis). As far as can be judged at present, better quality data was obtained with pinhole illumination, since the pinhole scattering amplitude seems to add coherently to the sample amplitude, thereby enhancing the signal. Using slits, spurious (imperfect) slit scattering dominated on the orthogonal axes and in the central region, spoiling the information in the corresponding pixels (in particular at low q).*

Göttingen group: During the period of the report, the Göttingen group has addressed the following work packages and has achieved the following goals:

- Preparation of focused ion beam (FIB) test samples for CDI
- use focused ion beam (FIB) for treatment of CDI pinholes
- preparation of high transmission waveguides based on a two-component cladding
- implementation and test of plunge freezing for vitrification of biological cells
- CDI experiment on (i) freeze dried and (ii) cryogenically vitrified bacterial and eukaryotic cells
- Design and test of 3-pinhole illumination system and instrumentation for CDI
- Construction and commissioning of optical test bench for CDI (based on 632 nm He NE laser)

HASYLAB group: The HASYLAB group has actively pursued coherent imaging experiments both at synchrotron beamlines as well as at FLASH, and has worked on reconstruction and algorithms.

The results of the PSI/cSAXS experiment 11/2007 were analyzed in collaboration between the different teams of the VI. Johannes Gulden from the HASYLAB team has obtained results on the reconstruction of the pinhole illumination function, see Figure 2.

***Figure 2**: 4 best reconstructions of pinhole9 (approx.8um) after 1950 it. All phases set to .*

Dresden Group: The Dresden Group has performed a CDI experiment using a (coherently) focussed beam by compound refractive lenses. Placing an Au nanocrystal (size ca. 90 nm) shown in Fig. 3(a) in the focus with a beam diameter of about 150 nm, far-field images with high fringe visibility could be collected [Fig. 3(b)]. In this way it was demonstrated that indeed diffraction-limited focusing yields a nanobeam with high lateral coherence (milestone 1 of coherent diffraction with nanobeam). From the diffraction pattern the gold sample was reliably reconstructed with a resolution of about 5 nm using the standard hybrid input-output algorithm [Fig. 3(c)]. The support constraint was set using the shrink-wrap algorithm (both algorithms were implemented in the *tomo* software package developed by C. Schroer and A. Schropp). The experiment demonstrates that in agreement with numerical simulations the wave front is flat in the focus and paves the way to a systematic combination of nanofocusing and coherent diffraction imaging.

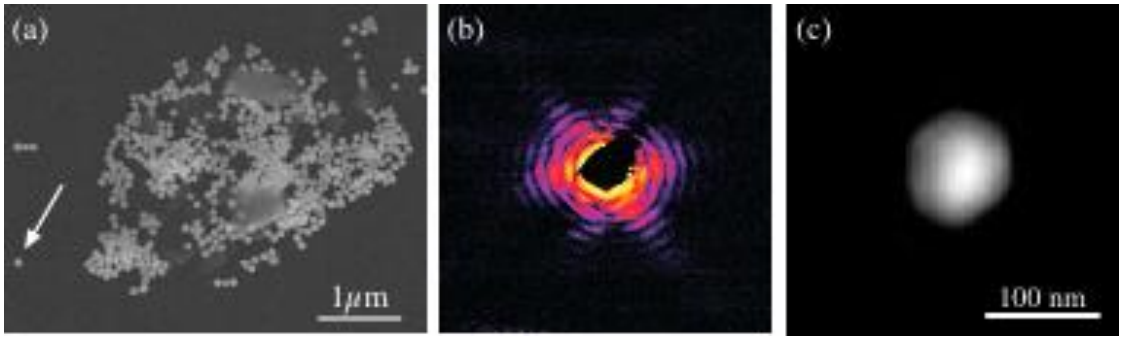

***Figure 3**: (a) Gold nanoparticles on Si_3N_4 membrane. The white arrow points to the gold particle under investigation. (b) Coherent diffraction pattern of the gold particle illuminated with a nanobeam with a diameter of about 150 nm. (c) Reconstructed gold particle.*

2.2 Research Activities in 4/2008-4/2009

Joint experiment at SLS

The analysis of the data from the joint beamtime during the previous report period at the coherent Small Angle X-ray Scattering (cSAXS) beamline of the Swiss Light Source (SLS) in Villigen, Switzerland, has led to the successful iterative reconstruction of a Siemens Star test pattern shown in Fig. 4(b).

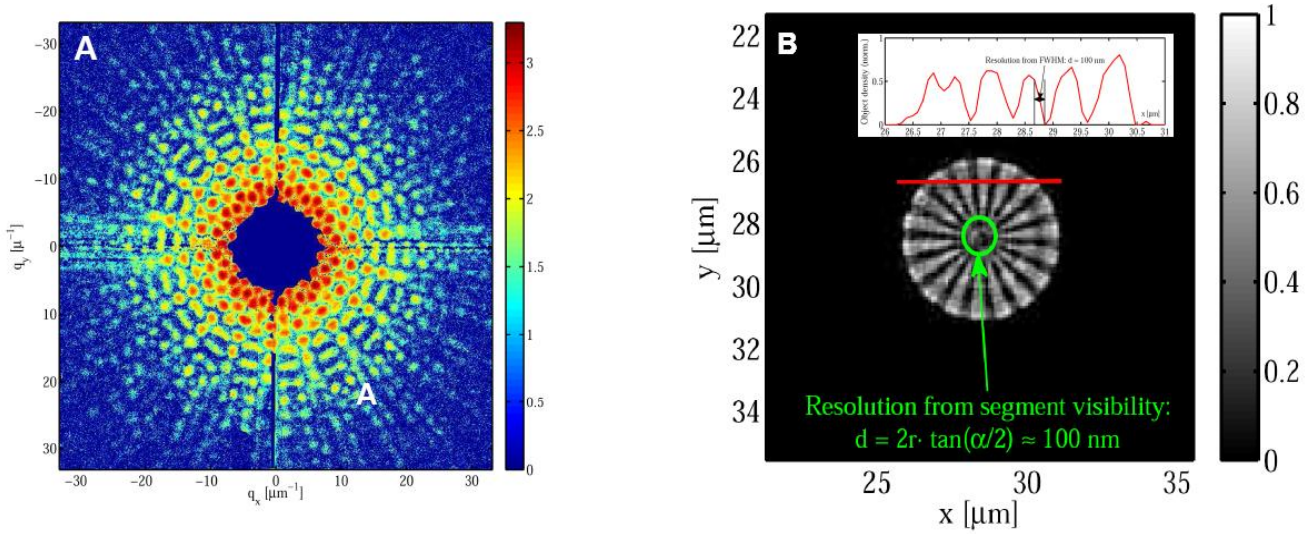

***Figure 4**: Coherent Diffraction pattern (A) and reconstructed amplitude (B) of a Siemens star test pattern after <100 iterations.*

The amplitude transmission function of the 40-nm-thick gold test pattern, which had been nano-fabricated with a Focused Ion Beam in the Göttingen group, could be reconstructed with a resolution of 100 nm, representing the first realization of Coherent X-ray Diffractive Imaging (CXDI) using the new PILATUS pixel detector. The corresponding diffraction pattern shown in Fig. 1A was collected using the classical setup for CXDI, using a near-plane-wave illumination defined by slits. For comparison, a pinhole wavefield propagated into the near field regime was also tested as an illumination function, however, a reconstruction was not successful due to limited knowledge about the full (complex) illuminating wavefield on the sample, which cannot be approximated by a plane wave, if the sample is positioned in the near field of the pinhole.

Preparing a joint experiment at ESRF

The team submitted a joint proposal entitled *Carbonate biomineralization in a living 'fossil': a structural approach by coherent diffractive imaging* at beamline ID13 of the ESRF. The proposal was accepted and received beamtime in July 2009. Preparations for this experiment have been made in all groups.

The aim of this experiment was to perform coherent diffraction imaging experiments, e. g., ptychographic scanning microscopy, with a hard x-ray nanobeam on biominerals. The beam was to be generated using nanofocusing refractive x-ray lenses at the new nanoprobe station at ID13. In preparation a refractive-lens unit for the nanoprobe was designed, built, and tested by the TU Dresden group at ID13 (see section below). First test experiments on biominerals were carried out using this setup. A fluorescence map with 100 x 100 nm^2 pixel size is shown in Fig. 5 (A). The scanned region belongs to a sample of ANME-2 (anaerobic-methane-oxidizing communities)/ gereigit (Fe3S4)- bearing DSS

(*Desulfosarcinales/Desulfobacterium*) consortia. The fluorescence mapping almost resolves the chains of precipitated ferrimagnetic greigit cristals which are visualized on a TEM image of the same region in Fig. 5 (B). It illustrates the high resolution achievable with the nanoprobe and that fluorescence data can be used to identify characteristic features in the sample.

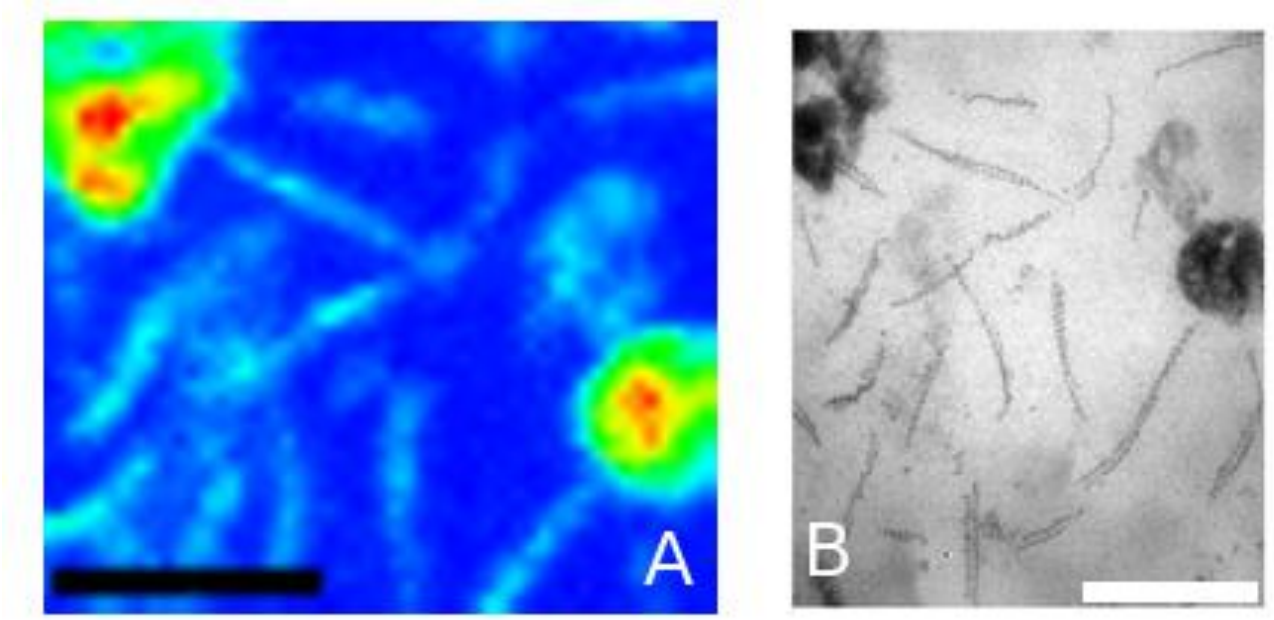

Figure 5*: (A) Fluorescence map of iron (K-alpha) in microbial mat recorded with the hard x-ray nanoprobe based on nanofocusing refractive x-ray lenses. (B) TEM image of the same region shown in (A). Scale bars denote 2 µm.*

Göttingen group: In a second experiment at the cSAXS beamline performed by the Göttingen group in November 2008 the previous efforts were continued, applying the new technique of Scanning X-ray Diffraction Microscopy (SXDM), which had been developed by the cSAXS research team in 2008 [1]. This allows for a simultaneous reconstruction of both the complex illumination function and the object transmission function. As a consequence, no approximations or idealizations of the illuminating wavefield are necessary any more. Using a very similar experimental approach as in the previous beamtime, the sample was illuminated by the near field of a pinhole. The SXDM technique involves the analysis of many diffraction patterns collected on a grid of scan points on the sample. Therefore the sample was scanned through the fixed illuminating wavefield during the experiment. As a first specimen a nano-fabricated commercial test pattern (NTT-AT, Japan) was used, and the corresponding object transmission function could be imaged with a resolution of 50 nm (see Fig. 6).

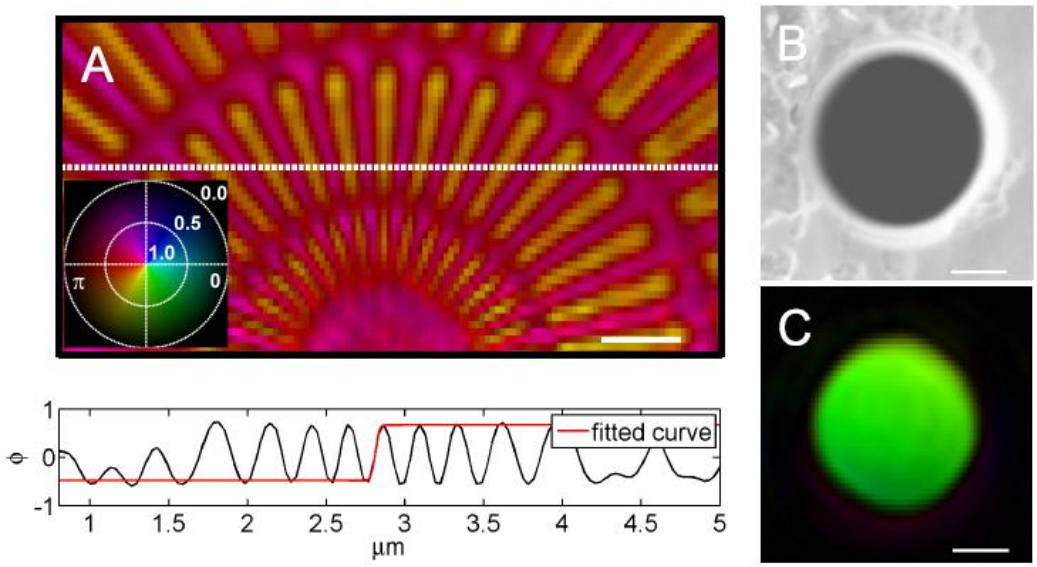

***Figure 6**: Reconstruction of the complex object transmission function (A) and the illuminating pinhole wavefield in the plane of the pinhole (C), obtained by SXDM. A scanning electron micrograph of the pinhole is depicted in subfigure B. A line cut through the phase distribution of the object transmission function yields a resolution of 50 nm. Scale bars denote 500 nm. (preliminary result)*

In a second step freeze-dried cells of the bacterium *Deinococcus radiodurans* were imaged with a resolution approaching 150 nm, applying the very low dose of $2 \cdot 10^3$ Gy (see Fig. 7).

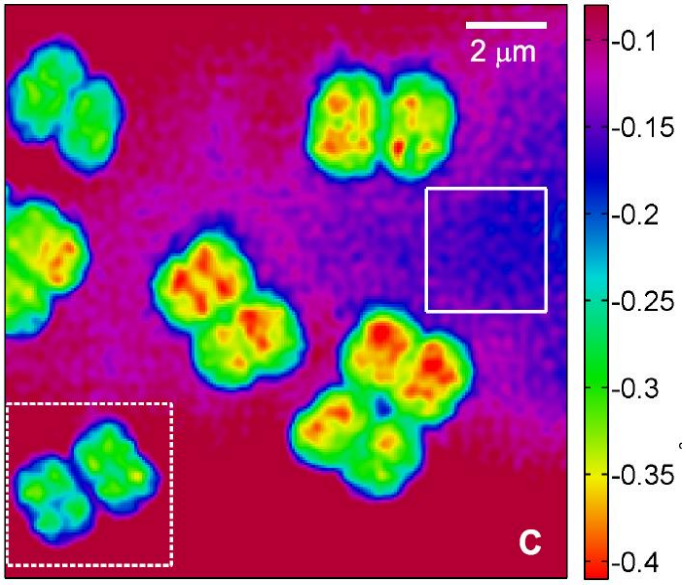

***Figure 7**: Reconstructed phase distribution corresponding to freeze-dried bacterial cells (Giewekemeyer et al., unpublished preliminary result)*

Due to the simple average composition of organic material and the kinematic scattering process at hard X-ray energies (6.2 keV was used here), the corresponding area mass density distribution can be extracted

from the reconstructed phase map. As visible in the reconstruction, internal features of the cells can be visualized. Compared to the experiment of Nov. 2007, several improvements of the experimental setup (optical online micrsocopy, improved pinhole with 1.4 micron diameter, optimization for stability) have made this result possible.

As similar datasets have been collected in the cSAXS beamtime of 2007, a further analysis of the obtained data with the newly available algorithmic tools was then possible and could possibly lead to a successful reconstruction of the diffraction patterns obtained with pinhole illumination described above. This path was, however, not followed later due to limited man power and an emphasis on the analysis of new data obtained with better detectors from the 2009 beamtime. The gained expertise on the algorithmic side was an essential prerequisite for the joint experiment at the ID 13 endstation of the ESRF in July 2009.

Quantitative simulations have been performed addressing the feasibility of hard X-ray holographic imaging of biological material, which acts as a weak, pure phase object in this photon energy regime.

As an independent approach towards holographic imaging a recently proposed scheme by Podorov et al. [2] for pure amplitude objects has been extended to the more relevant case of phase samples (see above) and demonstrated experimentally, for the first time, with visible light [3].

References

[1] Thibault, P. *et al.* Science **321**, 379 (2008)
[2] Podorov, S. G., Pavlov K.M. and Paganin D.M. Opt. Express **15**, 9954 (2007)
[3] Enders, B., Giewekemeyer, K., Kurz, T., Podorov, S., and Salditt, T., New J. Phys. **11**, 043021 (2009)

Dresden Group: In the previous reporting period a first CXDI experiment with nanofocused radiation had been performed. The coherent diffraction image of a single gold nanoparticle was reconstructed with the unprecedented spatial resolution of 5 nm [1]. This high resolution is possible due to the high flux density produced by nanofocusing onto the sample. Indeed, a dose density of $1.5 \cdot 10^6$ ph/nm^2 is required to record a high-resolution pattern of the gold particle that comprises about $1.6 \cdot 10^7$ atoms. With the same setup, a series of user experiments were carried out, e. g., a diffraction experiment from single SiGe islands grown on a silicon substrate [2].

In a follow-up experiment various instrumental components have been optimized, such as the nanofocusing lenses and the beamstop, and the whole experiment was performed at the new nanoprobe station at ID13. The latter has a significantly improved mechanical and thermal stability that is crucial, in particular for ptychographic scanning experiments. To reach highest spatial resolution, an optics block that fits into the nanoprobe setup (cf. Fig. 8) was designed and built in collaboration with the beamline. This optics block together with a new generation of nanofocusing lenses made of silicon was thoroughly tested in Feb. 2009. A series of test experiments were carried out with the setup, in particular, the fluorescence map shown in Fig. 5 was recorded.

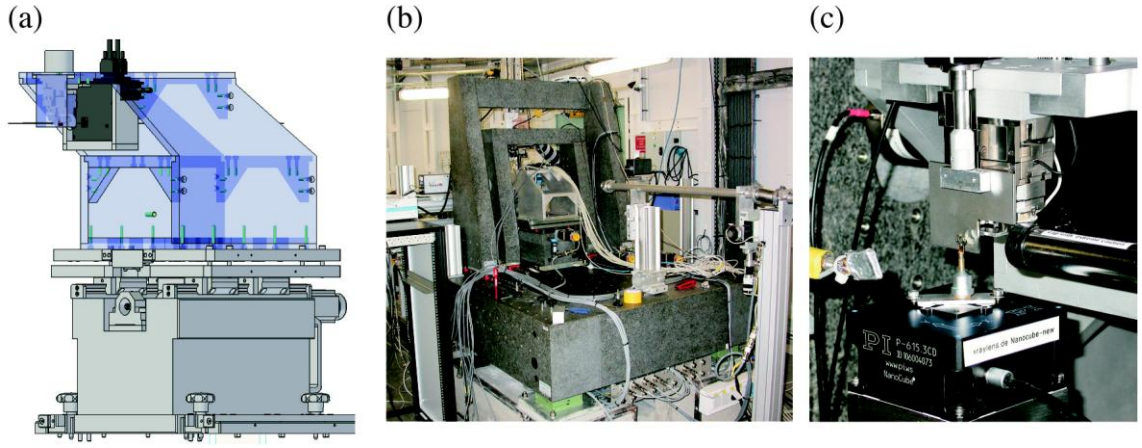

Figure 8: *(a) Design of the optics block for nanofocusing lenses at the nanoprobe station at ID13. (b) Optics block installed at ID13. (c) View of the sample behind the optics block.*

To verify the suitability of the setup for coherent diffraction imaging, a CXDI experiment with nanofocused radiation has been performed. In Fig. 9(a) a cluster of four small gold particles (~ 40 nm diameter, each, overall $7.5 \cdot 10^6$ atoms) is depicted that was illuminated by a hard x-ray nanobeam (E = 15.25 keV). Fig. 9(b) shows the diffraction pattern recorded of the cluster in 1200 s and Fig. 9(c) the reconstruction to about 10 nm. As the diffraction pattern is not point symmetric, the reconstructed object is complex. As such a small gold sample does not lead to a significant phase shift, the phase must be interpreted as coming from the illumination. This shows that the sample was not perfectly in focus or the focus was slightly distorted due to aberrations. Using ptychographic scanning techniques, the illumination could be separated from the object. The example shows that the latter is important to obtain quantitative information about the sample. In addition to conventional CXDI, a ptychogram of a test pattern from NTT-AT was performed.

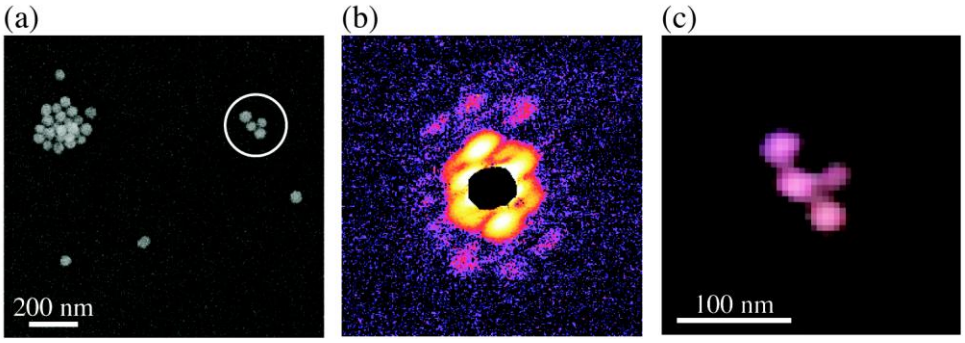

Figure 9: *(a) SEM image of gold particles (diameter approx. 40 nm) on a Si_3N_4 membrane. The circled cluster was illuminated with a hard x-ray nanobeam, producing the diffraction pattern shown in (b) after 1200 s of exposure. (c) reconstructed cluster of gold particles at around 10 nm resolution. (unpublished)*

Currently, the main limitation for CXDI techniques seems to be the detector. CCD cameras used in these experiments have non-negligible readout noise and dark current, and require the use of a beamstop to avoid spilling of electrons from overexposed pixels into neighboring ones. In addition, the FReLoN detector of ID13 seems not to be as sensitive as the one from ID11 used in the previous experiment [1]. Experience with photon counting pixel detectors (e. g., PILATUS 2M at cSAXS, SLS) shows that the improved data

quality from these detectors makes the algorithms converge much more reliably. In addition, overexposure is not critical for these detectors, as long as dead-time effects can be neglected. Therefore, for the 2009 joint experiment at ID13, a MAXIPIX detector was used.

In the reporting period, a series of reconstruction schemes wer implemented in the software developed by the group, including the reconstruction scheme for ptychographic imaging by Thibault, et al. [3]. Ptychographic reconstruction requires the exact knowledge of the positions of the illumination on the sample during the scan. This is a particular challenge for small illuminations and highest spatial resolutions. The redundance of an oversampled ptychogram, however, allows one to refine the positions of the illumination on the sample. A reconstruction scheme including small variations around the scanning positions in the ptychographic scan was published by Guizar-Sicairos and Fienup [4]. In order to be able to account for positioning inaccuracies at high spatial resolution, this latter scheme was implemented.

References

[1] C. G. Schroer, et al., Phys. Rev. Lett **101**, 090801 (2008).
[2] M. Hanke, et al., Appl. Phys. Lett., **92**, 193109 (2008).
[3] Thibault, P. *et al.* Science **321**, 379 (2008).
[4] M. Guizar-Sicairos, J. R. Fienup. Optics Express, **16**, 7264 (2008).

DESY group:

a) Coherent diffraction tomography of nanoislands from grazing-incidence small-angle x-ray scattering.

Tomography and especially x-ray tomography has become one of the most important tools for investigating three-dimensional (3D) structures in condensed matter [1] and the life sciences [2]. When projected absorption contrast or phase contrast are measured in conventional x-ray transmission tomography the achievable resolution is limited by the spatial resolution of the area detector that can be about one micrometer. Coherent x-ray diffraction imaging (CXDI) technique represents a possible solution to this dilemma [3]. As no lenses are required in this imaging technique it allows one, at least in principle, to overcome the resolution limits of conventional x-ray microscopy and to obtain diffraction-limited images of a sample using phase retrieval [4].

To obtain a 3D image of a non-crystallographic object in the forward scattering geometry by the CXDI technique it is usually mounted on a Si_3N_4 membrane and then rotated with a fixed azimuthal angular step (see inset (a) in Fig. 10). Unfortunately, in this approach not all angles for a full 3D scan are accessible due to the positioning of the object on a membrane. The remaining part of reciprocal space therefore cannot be used for tomographic reconstruction, resulting in a certain loss of features in the reconstructed images that are present in the original object. Instead, it we proposed to position a sample on a flat thick substrate and to perform tomographic scans by collecting successive coherent scattering diffraction patterns at different azimuthal positions of a sample in a grazing-incidence small-angle x-ray scattering (GISAXS) geometry [5] (see Figs. 10 and 11). With this approach there are no limitations on the angle of rotation. Consequently large areas in reciprocal space can be measured with sufficient resolution and without missing wedge. The feasibility of this approach was tested and proven by a number of simulations [6]. Here we report on the experimental realization of this coherent diffraction tomographic technique.

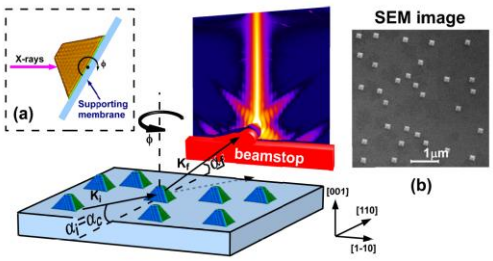

Figure. 10. *Schematic diagram of the GISAXS scattering geometry on a group of nano-islands in the form of a truncated pyramid with a square base. The incident wave vector* $\mathbf{k}_i$ *at grazing incidence angle* $\alpha_i = \alpha_c$ *and scattered wave vector* $\mathbf{k}_f$ *at angles* $\alpha_f \geq \alpha_c$ *are shown. The sample is rotated around the surface normal (azimuthal angles* ϕ*). Inset (a): Schematic diagram of a conventional CXDI tomography when the sample is positioned on a supporting membrane. (Inset (b)): A scanning electron microscopy image of the nano-islands.*

We used SiGe islands of 200 nm average base size grown by liquid phase epitaxy as model samples. All islands were coherently grown on a (001) Si surface and exhibit a truncated pyramidal shape with a square base (see inset (b) in Fig. 11). In addition, they exhibit a narrow size distribution (~10% full width at half maximum (FWHM)) and the same crystallographic orientation on the Si surface (Fig. 10).

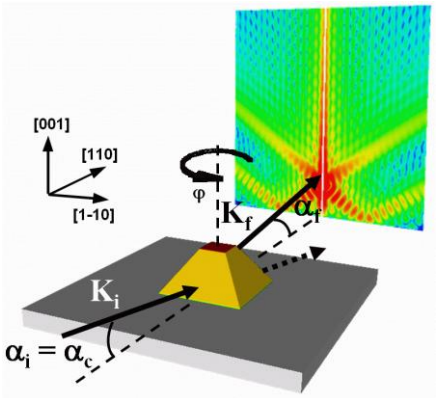

Figure 11: *An illustration of the coherent diffraction tomography technique in GISAXS geometry. Diffraction patterns are successively collected at different azimutal positions of the sample. The incidence angle of the x-ray beam is equal to the critical angle* $\alpha_i = \alpha_c$ *and is the same for all azimutal positions of the sample.*

Experiments were performed at the ID01 beamline of the European Synchrotron Radiation Facility (ESRF) in Grenoble. The incidence angle was taken equal to the critical angle for total external reflection of the Si substrate which corresponds to $\alpha_i = \alpha_c = 0.224°$ for the chosen x-ray energy of 8 keV. This particular angle was used because at these conditions the scattering may be considered as predominantly kinematical [7]. The coherently scattered signal was measured up to $q_{||} = \pm 0.56$ nm^{-1} in reciprocal space in the transverse direction. However, due to a certain noise level, only a limited part of reciprocal space up to $q_{||} = \pm 0.36$ nm^{-1} was considered for the reconstruction, which provides a 17.4 nm resolution in real space. An azimuthal scan was performed from –5° to 50° with an angular increment of 1°. Due to the four fold and mirror symmetry of {111} facetted islands such scans cover the whole reciprocal space. During the azimuthal scan the incidence angle was kept constant at the critical angle α_c.

The series of diffraction patterns at each azimuthal angle position represents slices through the 3D reciprocal space on a pseudopolar grid, and can be combined to produce a 3D intensity distribution in reciprocal space. An iso-intensity surface of this 3D representation of the scattered intensity is shown in Fig. 12(c). Strong crystal truncation rods (CTR) along the <111> directions and much weaker crystal truncation planes (CTP) connecting the CTRs can be observed [5]. For comparison we performed

calculations of GISAXS diffraction patterns in the framework of the distorted-wave Born-approximation (DWBA) theory for similar pyramids. The corresponding 3D representation of the scattered intensity is shown in Fig. 12(a). Strong interference fringes due to the coherent scattering of the x-ray beam from a small pyramid-shaped object can be observed in this figure. These interference fringes are smeared out in our experimental data (Fig. 12(c)) partly due to a finite size distribution of the islands and partly due to a lack of sufficient counting statistics. In order to model the experimental results we added a Gaussian mask to the calculated set of data. The corresponding 3D representation of the scattered intensity is shown in Fig. 12(b).

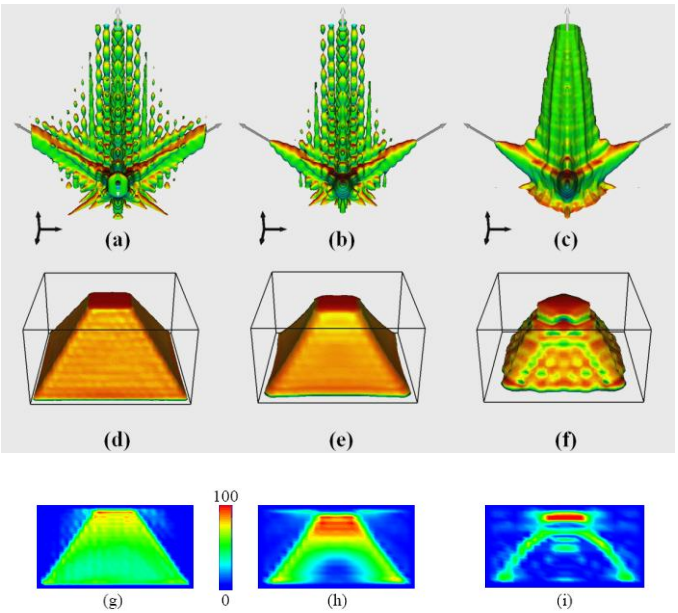

Figure 12:. *Left column [(a), (d), (g)]: simulations in the framework of the DWBA theory. Middle column [(b), (e), (h)]: simulations in the framework of the DWBA theory with an additional Gaussian mask (for details see text). Right column [(c), (f), (i)]: experiment. [(a), (b),(c)]: 3D plot of an iso-intensity surface in the reciprocal space. RGB colors correspond to the z-projection of the iso-surface normal. Grey arrows indicate directions along the crystallographic planes (001) top and {111} on the side. Black arrows indicate q_x, q_y, q_z directions in reciprocal space. The length of each black arrow corresponds to 0.1 nm^{-1}. [(d), (e), (f)]: Reconstructed shape of the islands. The transparent box indicates the size of the support. [(g), (h), (i)]: Electron density of the islands obtained as a vertical section through the center of each island.*

Results of the island shape reconstruction from the experimental GISAXS diffraction patterns are presented in Fig. 12(f). For comparison, results of the reconstruction of the island shape from simulated data are also shown in Fig. 12(d,e). The electron densities of the islands obtained as a vertical section through the center of the islands are presented in Figs. 12(g-i). From these results it is seen that the shape of the islands is reconstructed correctly for the experimental data set (Fig. 12(f)). However, for the electron density inside the island we observe artifacts in the form of low density regions in the bottom of the islands (Fig. 12(i)). Reconstructions performed with the simulated data sets show that the scattering data obtained in the DWBA conditions correctly reproduce the shape (Fig. 12(d)) and electron density (Fig. 12(g)) of an island. At the same time, when the modified theoretical data set with the Gaussian mask is used for reconstruction, artifacts similar to those from the experimental data set appear. These results suggest that the artifacts can be removed by an increased incidence flux (e.g. by using focusing optics) and with the use of a new generation of detectors with extremely high dynamic range.

In conclusion we have demonstrated how this approach of coherent diffraction GISAXS can be used to obtain the 3D electron density of nanometer sized islands. This was achieved by performing tomographic azimuthal scans in a GISAXS geometry on many identical islands and subsequent phase retrieval which yields the tomographic information, such as the shape and the electron density. It is important to note that this approach does not depend on the crystalline structure of such an island and may be applied to any material system. In our future work we are planning to extend this technique to map the variation of 3D electron density in nano-islands caused by the existence of a chemical composition gradient.

References

1. 1. *Advanced Tomographic Methods in Materials Research and Engineering*, (Ed. by J. Banhart, Oxford University Press, New-York, 2008).
2. C. A. Larabell, and M. A. Le Gros, Mol. Biol. Cell, 15 957 (2004) ; P. C. J. Donoghue, *et al., Nature* 442, 680 (2006).
3. J. Miao, *et al.,* Nature 400, 342 (1999) ; M. Pfeifer, *et al.,* Nature, 442, 63, (2006); D. Shapiro, *et al.,* Proc. Natl. Acad. Sci. U.S.A. 102, 15343 (2005);
4. J. R. Fienup, Appl. Opt. 21, 2758 (1982); V. Elser, J. Opt. Soc. Am. A 20, 40 (2003).
5. I. A. Vartanyants, A. V. Zozulya, K. Mundboth, *et al.,* Phys Rev. B 77, 115317 (2007).
6. O. M. Yefanov and I. A. Vartanyants, Eur. Phys. J. Special Topics 167, 81 (2009).
7. I. Vartanyants, D. Grigoriev, A. Zozulya, Thin Solid Films 515, 5546 (2007).

Original publication

O. M. Yefanov, A.V. Zozulya, I.A. Vartanyants, *et al.,*"Coherent diffraction tomography of nanoislands from grazing-incidence small-angle x-ray scattering", Appl. Phys. Lett. **94**, 123104 (2009).

b) Coherent-pulse 2D Crystallography at Free-Eelectron Lasers.

Revealing the structure of protein molecules is mandatory for understanding the structure of larger biological complexes. The major progress in uncovering the structure of proteins in past decades was due to the development of phasing methods [1] allowing the determination of the structure of complex molecules that crystallize. In spite of considerable progress in macromolecular crystallography, crystallization and radiation damage is still a bottleneck in protein structure determination. One new approach to overcome these difficulties is based on the use of ultrashort pulses of x-ray free-electron lasers (XFEL) [2]. An elegant idea is based on measuring a sufficiently sampled diffraction pattern from a single molecule illuminated by an FEL pulse [3]. However, in spite of the extreme intensity of the FEL pulses, a diffraction pattern from only one molecule will not be sufficient to obtain a high resolution diffraction pattern. Many reproducible copies will need to be measured to get a sufficient signal to noise ratio for each projection necessary for three-dimensional (3D) imaging at sub-nanometer spatial resolution. Alternatively, we propose to use two-dimensional (2D) finite crystals to reveal the structure of single molecules. This can be especially important for the membrane proteins that in general do not form 3D crystals, but easily form 2D crystalline structures.

Free-electron lasers are especially well suited for such coherent 2D crystallography. They provide femtosecond coherent pulses with extremely high power. Only the combination of all of these unique properties will allow the realization of 2D crystallographic x-ray imaging on biological systems. Brilliant,

ultrashort pulses could overcome the radiation damage problem [3] which is a severe limitation of conventional crystallography at 3rd generation synchrotron sources [4]. Higher luminosity and hence improved statistics for such experiments can be obtained by the use of pulse trains that can be provided by FLASH [5].

We demonstrate finite crystallography by using a micro-structured crystal array that was prepared on a 100 nm thick silicon nitride membrane substrate coated with 600 nm of gold, and 200 nm of palladium. The finite crystal sample was manufactured by milling holes in the film in a regular array pattern using a Focused Ion Beam (FIB). The 'unit cell' of our crystal consists of a large hole of 500 nm diameter (representing a 'heavy atom' in conventional crystallography) and a smaller hole of 200 nm diameter (representing a 'light atom'). The whole structure is composed of five unit cells in each direction, making the total structure size about 10 μm x 10 μm.

The diffraction data were measured at FLASH on the PG2 monochromator beamline [6] with a fundamental wavelength of 7.97 nm. The scheme of experiment is shown in Fig. 13.

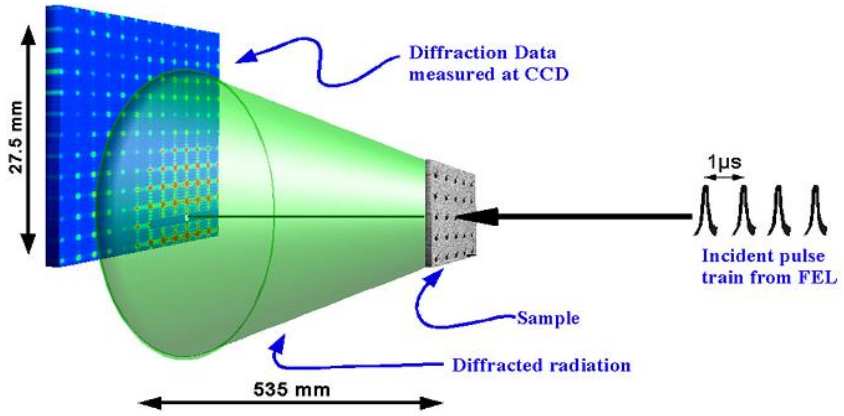

***Figure 13**: A sketch of the experiment. The beam from the beamline first interacts with the sample, and then the diffracted radiation propagates to a CCD detector. To enhance the measured resolution of the data the direct beam was incident near the corner of the detector.*

We used a 0.2 s exposure time to collect a series of single pulse train data from our sample with a coherent flux on the sample area of 1.5×10^{10} photons per pulse train. This is an order of magnitude higher than the expected coherent flux of about 3×10^{9} photons on the same sample area for the same exposure time at a 3rd generation synchrotron source. A typical data set is shown in Fig. 14(a). The diffraction pattern as measured contains signal up to the edge of the detector, which corresponds to a minimum feature size of 220 nm (Fig. 14(a)). We note that all expected features of a finite, crystalline structure are observed. The Bragg peaks due to the regular array are clearly seen, as are the oscillations between the Bragg peaks that are the result of the finite extent and coherent illumination of our sample. Also seen is the form factor from the individual elements – the large holes – that can be observed as a radial intensity modulation across the pattern produced.

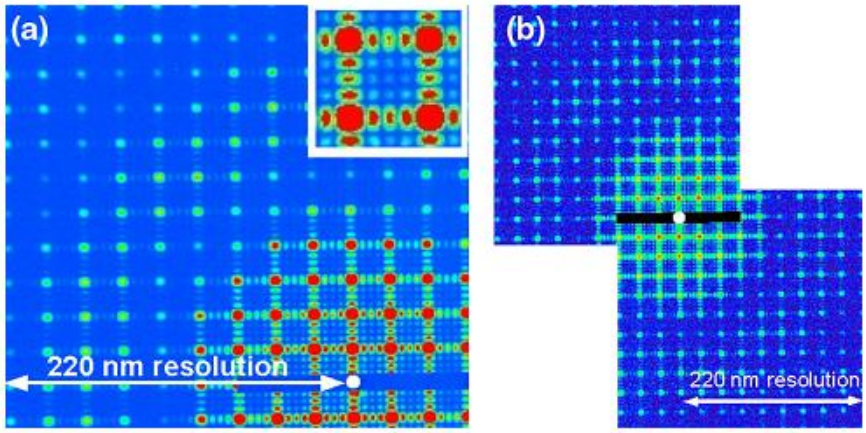

***Figure 14**: (a) Far-field diffraction data measured from a single train of 21 femtosecond pulses from the FEL. (Inset) Enlarged region of diffraction pattern. (b) A symmetrized version of (a) used for reconstruction. The region in black corresponds to missing data covered by the beamstop. The white dot (in both panels) corresponds to the center of the incoming beam.*

The preprocessed data set (shown in Fig. 14(b)) was used for reconstruction by applying the Hybrid Input-Output (HIO) iterative phase retrieval algorithm [7]. A scanning ion micrograph (SIM) image of the object under investigation is shown in Fig. 15(a). The initial square support used for reconstruction is indicated by a dashed line in Fig. 15(b). It is very clearly seen in Fig. 15(c) that the periodic array of large holes are successfully reconstructed, however the small holes of 200 nm diameter are missing. Note also the diffuse, elongated background present in the reconstruction.

Our analysis has shown that one of the reasons for the limited resolution and its sensitivity to noise obtained in our initial reconstructions is due to the fact that the measured diffraction pattern has two equivalent, symmetric solutions. One is with the small dots appearing to the top right of the larger dots, and the other is with them appearing to the bottom left. Due to this symmetry the reconstruction algorithm does not fully converge, but rather stagnates with two equivalent solutions superimposed with each other. To solve this problem we have binned the data 5x5 (yielding a sampling rate of 6 in each dimension). In addition, instead of using a large square support we used a more constrained support of 25 rectangular boxes each centered on the positions of the unit cell (see Fig. 15(b)). By improving the noise statistics and reducing the symmetry in real space we were able to improve the reconstruction to the level that we resolved the smallest features present in our sample (Fig. 15(d)). Our analysis has shown that the obtained resolution in real space was better than 238 nm. This compares favorably with our measured maximum momentum transfer that corresponds to 220 nm resolution (see Fig. 14).

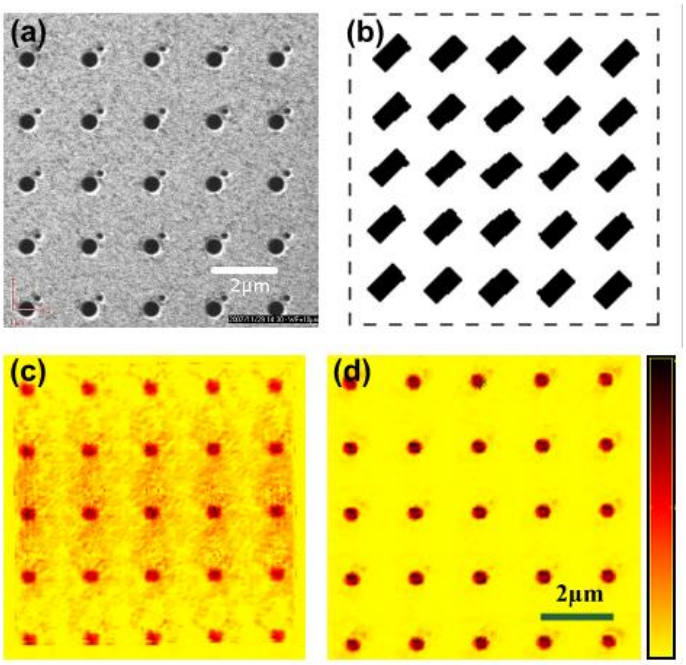

Figure 15: *a) SIM image of the finite, periodic structure. (b) Support region used for the reconstruction of the diffraction pattern. The large rectangular support (dashed line) was used in the reconstruction shown in (c). The support in the form of 25 rectangular boxes was used in the reconstruction shown in (d). (c) The initial reconstructed image with the original data binned 3x3. (d) The final reconstructed image of the sample using the original data binned 5x5 and exhibiting a resolution as measured in the experiment.*

In summary, we have demonstrated single pulse train coherent diffractive imaging for a finite crystalline sample with the reconstructed image exhibiting resolution commensurate with the maximum momentum transfer measured in the diffraction data. Furthermore, we demonstrate that the traditionally non-crystalline framework of coherent diffractive imaging is applicable to two-dimensional finite crystals. In this experiment the 2D crystalline structure has been essential in providing the necessary signal to determine the structure of the unit cells. If only a single unit cell were used simulations suggest that a successful reconstruction to the resolution shown here would be impossible. These findings improve the scope of the fast growing technique of coherent imaging by including finite 2D crystalline specimens in the sphere of applicability of CXDI, and by utilizing these crystals to improve signal to noise, and hence resolution of CXDI reconstructed images. We conclude that this alternative approach to single molecule imaging is a significant step towards revealing the structure of proteins with sub-nanometer resolution at the newly built XFEL sources.

References

1. M.Woolfson & F. Hai-fu, *Physical and non-physical methods of solving crystal structures*, (Cambridge University Press, Cambridge, 1995).
2. Arthur J. *et al.* http://www-ssrl.slac.stanford.edu /LCLS/CDR/; Tanaka T. and Shintake T. http://www-xfel.spring8.or.jp/SCSSCDR.pdf; Altarelli, M. et al., http://xfel.desy.de/tdr/index_eng.html.
3. R. Neutze, R. Wouts, D. Spoel, E. Weckert and J. Hajdu, Nature **406**, 752 (2000).
4. C. Nave, E. F. Garman, J. Synchrotron Rad., **12,** 257 (2005).
5. W. Ackermann *et al.*, Nature Photonics **1,** 336 (2007).
6. M. Wellhoefer, *et al.*, J. Opt. A: Pure Appl. Opt. **9,** 749 (2007).
7. J. R. Fienup, Appl. Opt. **21**, 2758 (1982).

Original publication
A.P. Mancuso[1], A. Schropp[1], B. Reime[1], *et al.,* "Coherent-pulse 2D Crystallography at Free Electron Lasers" Phys. Rev. Lett. **102**, 035502/1-5 (2009).

c) Transverse-Coherence Properties of the Free-Eelectron Laser FLASH.

Coherence is one of the most prominent features of laser sources. With the advent of Free Electron Lasers (FEL) based on the Self Amplified Spontaneous Emission (SASE) principle [1] the possibility of building coherent sources with x-ray wavelengths has become feasible [2]. The measurement of the coherence properties of existing FELs is of vital importance for understanding the physical principles that lie behind the SASE generation of coherent beams, for optimization of the parameters of these sources, and for the construction of beamlines. These measurements are also important for planning future experiments on these sources that exploit the coherent properties of high power FEL beams. In future when x-ray FELs, with a unique femtosecond time structure, will become available this approach can even be used for different applications in materials science [3] and biology including such exciting possibilities as single molecule imaging [4].

Young's double slit experiment is one of the most efficient and widely used methods for measuring the transverse coherence properties of the wavefields. In our experiments we have used the same approach and performed double slit experiments to analyze the transverse coherence properties of FLASH (Free-electron LASer in Hamburg) [5].

The second order correlations of the wave fields are described in the theory of coherence by the mutual coherence function (MCF) $\Gamma_{12}(\tau)$, that defines the correlations between two complex values of the electric field $E(\mathbf{r}_1,t)$ and $E^*(\mathbf{r}_2,t+\tau)$ at different points $\mathbf{r}_1$ and $\mathbf{r}_2$ and separated by the time interval τ

$$\Gamma(\mathbf{r}_1, \mathbf{r}_2, \tau)=\langle E(\mathbf{r}_1,t) E^*(\mathbf{r}_2,t+\tau)\rangle \quad , \qquad (1)$$

where the brackets <> indicate the ensemble average. Correlations of the field in the spatial-frequency domain are determined by the cross-spectral density function (CSD) $W(\mathbf{r}_1, \mathbf{r}_2, \omega)$, which is a Fourier transform of the MCF

$$W(\mathbf{r}_1, \mathbf{r}_2,\omega)=\int\Gamma_{12}(\tau)e^{-i\omega\tau}d\tau. \qquad (2)$$

The spectral density of the field $S(\mathbf{r},\omega)$ is defined as the CSD function taken at the same position $S(\mathbf{r},\omega)=W(\mathbf{r}, \mathbf{r},\omega)$. The normalized versions of the two functions (1) and (2) are the complex degree of coherence $\gamma(\mathbf{r}_1, \mathbf{r}_2,\tau)$ and the spectral degree of coherence $\mu(\mathbf{r}_1, \mathbf{r}_2,\omega)$, respectively.

It has been shown [6], that under very general conditions, one can represent the CSD of a partially coherent statistically stationary field of any state of coherence as a sum of independent coherent modes $W(\mathbf{r}_1, \mathbf{r}_2,)=\sum_{j=0}\beta_j E_j^*(\mathbf{r}_1)E_j(\mathbf{r}_2)$, where β_j and $E_j(\mathbf{r}_2)$ are the eigenvalues and eigenfunctions. For our purposes it is especially important to calculate correlation functions at different distances from the source. These values of the CSD can be obtained at different distances by propagation of the individual coherent modes. Due to statistical independence of the modes the CSD after propagating a distance z is given as a sum of propagated modes $E_j(\mathbf{r},z)$ with the same eigenvalues β_j

$$W(\mathbf{r}_1, \mathbf{r}_2,z)=\sum_{j=0}\beta_j E_j^*(\mathbf{r}_1,z) E_j(\mathbf{r}_2,z). \qquad (3)$$

We used this approach to make a realistic and simple estimate of the coherence properties of the existing FLASH source that was modeled as a Gaussian Schell-model (GSM) source. For calculations we take parameters of FLASH as reported in [5] at a fundamental wavelength of 13.7 nm. The CSD was calculated at a distance 20 m downstream from the source using Eq. (3). Seven modes were used for that calculation. In Fig. 16 results of these calculations are presented. An analysis of the obtained results shows that for the parameters of FLASH a small number of transverse modes contribute to the total field (Fig. 16c). The second mode is about 40% of the fundamental, and the contribution of the sixth mode is more then two orders of magnitude smaller than the fundamental. As a consequence this demonstrates that our model source is not fully coherent (contribution of each mode to the spectral degree of coherence is shown in Fig 17). Analysis of the obtained results also gives the value of the transverse coherence l_c=715 μm 20 m downstream from FLASH.

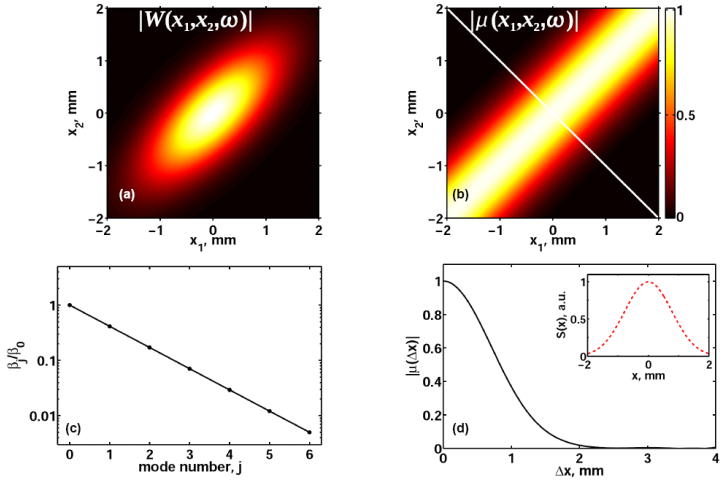

Figure 16 *(a) Modulus of the cross spectral density $|W(r_1, r_2)|$. (b) Modulus of the spectral degree of coherence $|\mu(r_1, r_2)|$. (c) The ratio β_j/β_0 of the eigenvalue β_j to the lowest order eigenvalue β_0 as a function of mode number j. (d) Modulus of the spectral degree of transverse coherence $|\mu(\Delta x)|$ taken along the white line in (b). In the inset spectral density S(x) is shown.*

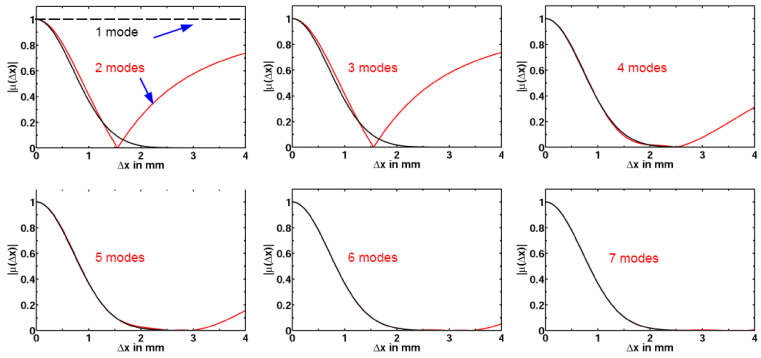

Figure 17: *Contribution of individual modes to the modulus of the spectral degree of coherence. Seven modes are sufficient to describe coherence properties at FLASH.*

The transverse coherence was measured using a double-slit experiment (see Fig. 18 (a)) at a fundamental wavelength of 13.7 nm during the commissioning phase of FLASH. The experiment was performed with a set of horizontal and vertical slits that was positioned at the distance z_1=20 m downstream from the last operating undulator module in the FEL tunnel. The distance d between the slit centers was 150, 300 and 600 μm for both vertical and horizontal pairs. The detector was located at a distance z_2=4.44 m downstream from the slit mask. Each interference pattern measured in this experiment was a result of the accumulation of ten bunches of a single train of FEL radiation. Each measurement for a given slit

separation was repeated ten times. The typical interference pattern measured on the detector with a horizontal slit separation of 150 μm is shown in Fig. 18 (b).

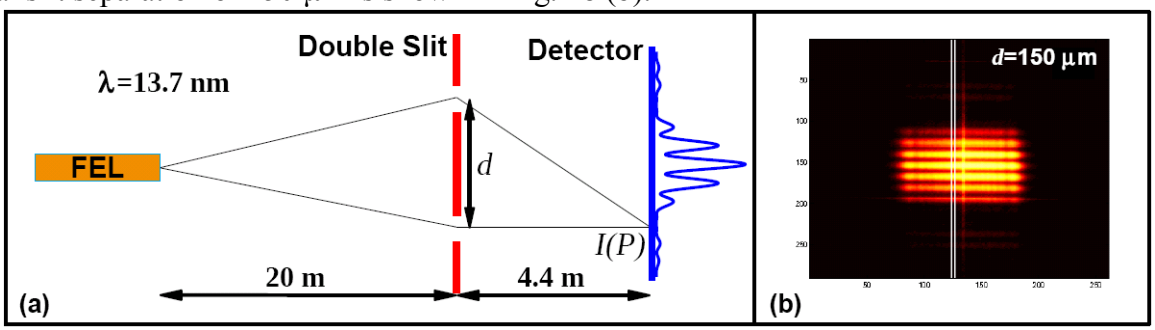

Figure 18: *(a) Scheme of the Young's double slit experiment performed at FLASH. (b) A typical interference pattern measured with the horizontal slits.*

All series of the experimental data were fitted to the following expression [7]

$$I(P) = I_1(P)+I_2(P)+2\sqrt{I_1(P)I_2(P)}\,|\gamma_{12}(\tau)|\cos[\omega\tau-\alpha_{12}(\tau)], \qquad (4)$$

where I_1(P) and I_2(P) are intensities at P corresponding to propagation of radiation from each of the slits separately, τ is the time delay for the radiation to reach point P at the detector from slits one and two and α_{12} (τ) is the relative phase. Typical results of the fit for different slit separations are shown in Fig. 19(a,b). As a result of the fitting the absolute value of the complex coherence factor $|\gamma_{12}|$ was obtained for each slit separation for both the horizontal and vertical directions (see Fig. 15 (c)).

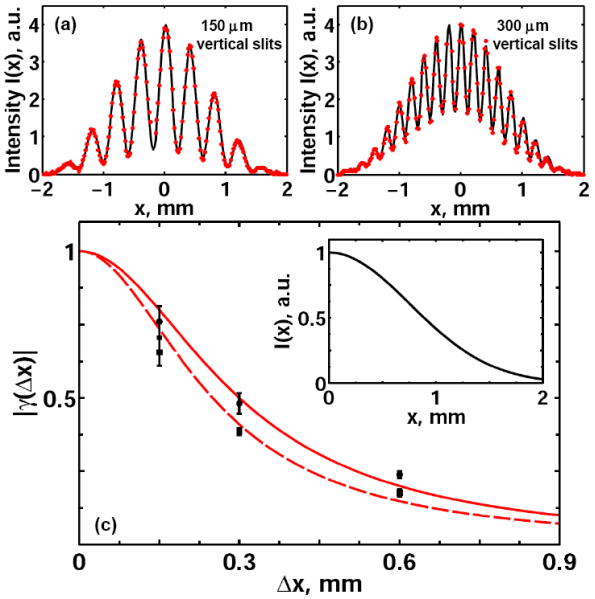

Figure 19: *(a),(b) Results of the fit (solid lines) to experimental data (dots) for different slit separation in the horizontal direction. (c) Modulus of the complex degree of coherence as function of slit separation in the horizontal (circles) and vertical (squares) directions obtained as a result of the fit to experimental data. Lorentzian fit to obtained values of $|\gamma(\Delta x)|$ is shown by solid (vertical direction) and dash (horizontal direction) lines. The intensity distribution is shown in the inset.*

Close inspection of the obtained results (Fig. 19) shows the following. First, it is clear that the radiation field is not fully coherent but is rather reduced at a few hundred microns length scale. This was already expected from our mode analysis of the radiation field with FLASH parameters. However, a

comparison with our previous calculations (see Fig. 16(d)) shows that the measured values of the degree of coherence for different slit separations is considerably lower than ultimately predicted by the model. The obtained values of the degree of coherence can be approximated by a Lorentzian function with the coherence lengths l_c(H)=300 μm in horizontal and l_c(V)=250 μm in the vertical directions. Obtained results are in very good agreement with the apparent source size observed with the wave front sensor at similar operating conditions of FLASH (it was about 2.5 times larger than reported in [5]).

In summary, we presented a theoretical and experimental analysis of the coherence properties of FLASH at a fundamental wavelength of 13.7 nm. We used a very general statistical optics theory to model the mode structure and coherence properties of the beam. With this approach the spectral density distribution as well as the complex degree of coherence can be calculated at any distance from the source with just a few input parameters. This very general modelling can be applied as an effective and useful tool for describing the coherence properties of SASE FELs. This approach may also be conveniently extended in future to calculate the coherence properties of FEL beams passing through different optical elements. Our analysis shows that FLASH is a highly coherent source which can be well described by a few coherent modes. We also performed a detailed analysis of the double slit measurements at FLASH which showed that the values of the degree of coherence are similar for the horizontal and vertical directions, and the coherence lengths are about three hundred microns at a distance 20 m downstream from the source.

References

1. E.L. Saldin, E.A. Schneidmiller, M.V. Yurkov, The Physics of Free Electron Lasers, (Springer-Verlag, Berlin, 2000).
2. Arthur J. *et al.* http://www-ssrl.slac.stanford.edu /LCLS/CDR/; Tanaka T. and Shintake T. http://www-xfel.spring8.or.jp/SCSSCDR.pdf; Altarelli, M. et al., http://xfel.desy.de/tdr/index_eng.html.
3. I. A. Vartanyants, I. K. Robinson, I. McNulty, *et al.,* J. Synchrotron Rad. **14**, 453 (2007).
4. R. Neutze, R. Wouts, D. Spoel, E. Weckert and J. Hajdu, Nature **406**, 752 (2000).
5. W. Ackermann *et al.*, Nature Photonics **1,** 336 (2007).
6. L. Mandel and E. Wolf, *Optical coherence and quantum optics* (University Press, Cambridge, 1995).
7. J.W. Goodman, *Statistical Optics* (Wiley, New York, 1985).

2.3 Research Activities in 5/2009-end of project

Joint experiment at ID13 / ESRF July 2009

The team performed a joint experiment entitled *Carbonate biomineralization in a living 'fossil': a structural approach by coherent diffractive imaging* at the ID13 Microfocus Beamline of the ESRF. The proposal received beamtime in July 2009. The first aim of this experiment was to perform coherent diffraction imaging experiments, e. g., ptychographic scanning microscopy, with a hard x-ray nanobeam on biominerals. The nanobeam was generated using nanofocusing refractive x-ray lenses at the new nanoprobe station at ID13. In preparation, a refractive-lens unit for the nanoprobe was designed, built, and tested by the TU Dresden group at ID13. The fluorescence signal of the specimen was collected parallel to the diffraction patterns.

Coherent X-ray Diffraction Imaging (CXDI) data sets have been collected on test patterns as well as on biomineralized carbonate and greigite specimens and biological samples. The spherulites of the coralline demisponge of *Astrosclera willeyana*, symbiotic asscociations of methanogenic archaea and sulfate reducing eubacterian, namely ANME-2 (anaerobic methane-oxidizing archaea)/ greigite-bearing *Desulfosarcina/ Desulfococcus* group (DSS), unstained freeze-dried cells of the bacterium *Deinococcus*

radiodurans as well as a simple Pollen have been studied at 15.25 keV photon energy in different imaging modes.

In the first part of the experiment ptychographic CXDI was applied to a lithographic test structure in order to retrieve the illuminating wave field and the wave field of the test chart down to a spatial resolution of a few tenth of nanometres (cf. Fig 20 for reconstruction of the test structure). The setup was such that the sample was placed in the focal plane. No beamstop was used. The illumination function yielded a very accurate and detailed picture of the focusing optics which consisted of a pair of refractive X-ray silicon lenses [1]. Beside obtaining the wave field of the sample we recorded simultaneously high resolution fluorescence data of the very same part of the Tantalum test structure.

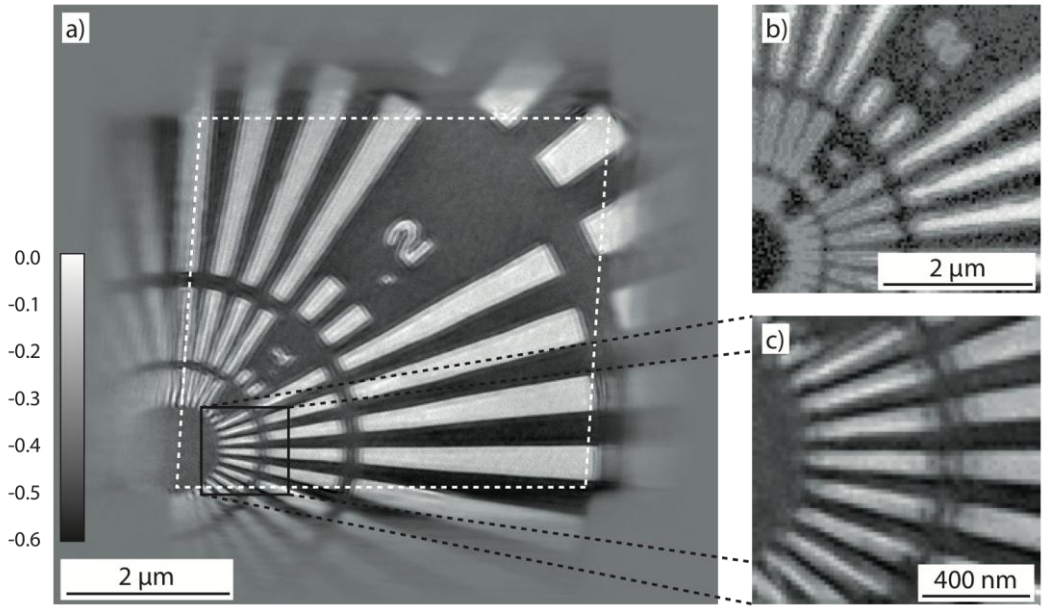

Figure 20: *a) Phase of the reconstructed transmission function of the object. The grayscale legend refers to values measured in radians. The expected phase shift of -0.46 radian is in good agreement with the reconstruction. b) Fluorescence map (Ta L-radiation) of the scanned area. c) Detail view of the region marked by the black square in a).*

In the second part of this experiment various ptychographic CXDI data sets of the declared specimens were collected. Again, the measurements have been supported by fluorescence scans in parallel. In addition to the fluorescence data information we used the ptychographic CDI data sets to directly obtain high resolution images of different contrast schemes, e.g. differential phase contrast (DPC) and darkfield (DF) (cf. Fig. 22 *A. willeyana*). Note, that the sample had to be moved into defocus for larger specimen like *A. willeyana*.

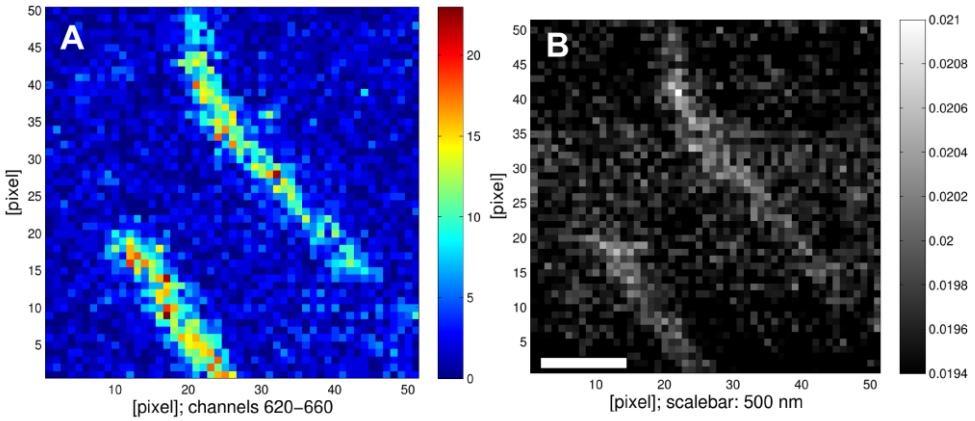

Figure 21:*-(bottom) (A) Fluorescence map (Fe K-shell) of two chains of magnetosoms. (B) Darkfield image from the same region. Exposuretime was 1s for each pixel. A 2.5 mm beamstop was used. The scalebar denotes 500 nm.*

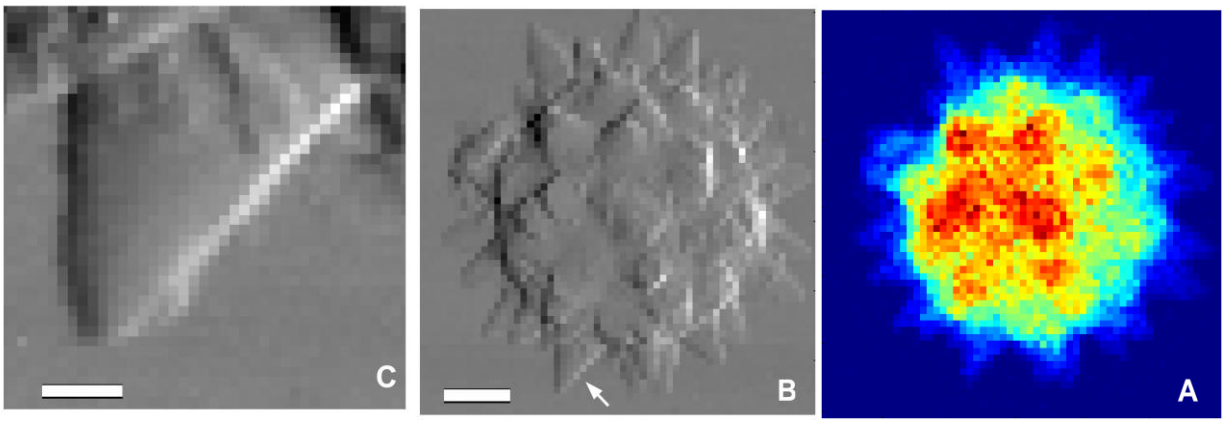

Figure 22:*-(top). Astrosclera willeyana: (A) Fluorescence map (Ca K-shell). (B) Phase contrast image at 0.5 mm defocus from the same region of (A). The scale bar denotes 5 µm (C) Phase contrast image at 0.25 mm defocus from a detail (white arrow) of (B) . The scale bar denotes 1 µm.*

Göttingen Group:

Quantitative biological imaging by ptychographic x-ray diffraction microscopy

We have carried out a first application of ptychography to the biologically relevant case of weakly scattering cellular material. Quantitative phase maps with a phase resolution below 1%π have been reconstructed from diffraction data of unstained freeze-dried cells of the gram-positive bacterium *Deinococcus radiodurans* (see Fig. 23). In contrast to previous CXDI experiments on biological objects, the sample did not need to be isolated and a quantitative result of high quality was obtained within comparatively short illumination time using a mildly-focused multi-keV synchrotron X-ray beam. Quantitative area electron density maps of the cellular structure could be extracted from the reconstructed 2D phase distribution. This opens up a complementary approach to recent electron microscopy studies of the bacterial nucleoid in *D. radiodurans*. The key question of these studies aims at unraveling possible correlations of the bacterium's extraordinary resistance to high doses of ionizing radiation and the structural arrangement of its nucleoid.

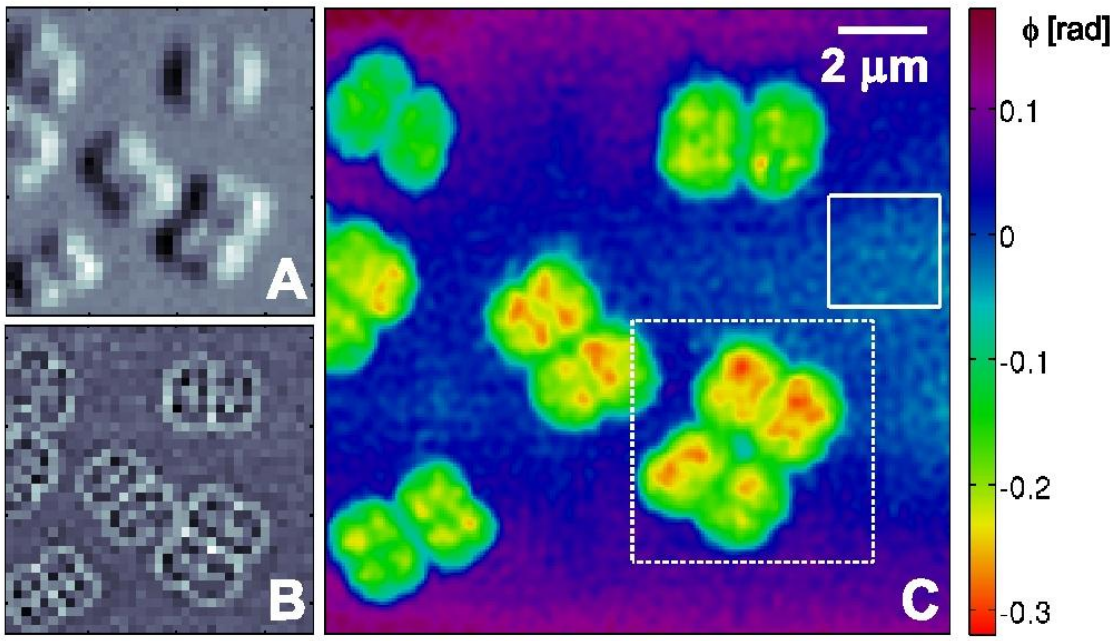

Figure 23:. *Scanning Xray Diffraction Microscopy of freeze-dried D. radiodurans cells. (A) Differential phase contrast image of a subset of the scanned region. One pixel corresponds to one scan point (pixel size is 400 x 400 nm). (B) Dark field contrast image of the same region as shown in A. (C) SXDM reconstruction of the object transmission function (phase) in the same region as shown in A and B. In the areas without cells statistical phase fluctuations are visible, the standard deviation of the phase distribution within the solid rectangle is 0.013 rad. Figure from [1].*

Lensless biological x-ray microscopy using waveguides

In an experiment at ID22 of ESRF, the Goettingen team has used x-ray waveguides as highly-confining optical elements for nanoscale imaging of unstained biological cells using the simple geometry of in-line holography. Holographic projection imaging with multi keV x-ray radiation in combination with tomographic reconstruction has a unique potential for lensless 3D image reconstruction, bringing together the earlier concepts of geometric magnification by a divergent beam and the principle of in-line holography. The well-known twin-image problem was effectively circumvented by a simple and fast iterative reconstruction. The algorithm was optimized for phase contrast transparent samples, well justified for multi-keV photon energies. The experimental scheme allows for a quantitative phase reconstruction from a single holographic image without detailed knowledge of the illumination function incident on the sample, as demonstrated for freeze dried cells of the eukaryotic amoeba *Dictyostelium discoideum* (see Fig. 24).

The sample can be reconstructed as in reference-beam holography by a direct (single-step) backpropagation. However, the image quality is severely limited by the well-known twin image problem of (in-line) holography. Experimental remedies used in the past include the recording of multiple holograms at various detector-to-sample positions, or an exact knowledge of the illumination function, both followed by iterative phase retrieval. We have shown that the quasi-spherical wave front exiting from a 2-dimensional x-ray waveguide (WG) can be used advantageously for holographic image recording from an unstained biological cell, followed by a robust and quickly converging iterative image reconstruction scheme from a single holographic image. The very high beam confinement substantially below 20 nm, which is possible using new-generation x-ray waveguides, leads to stable reconstructions for weakly

scattering biological objects without exact knowledge of the illumination function, even in the presence of intensity fluctuations. The method is well-adapted for the experimental situation of an essentially pure phase contrast specimen, and takes photon noise effects into account quantitatively.

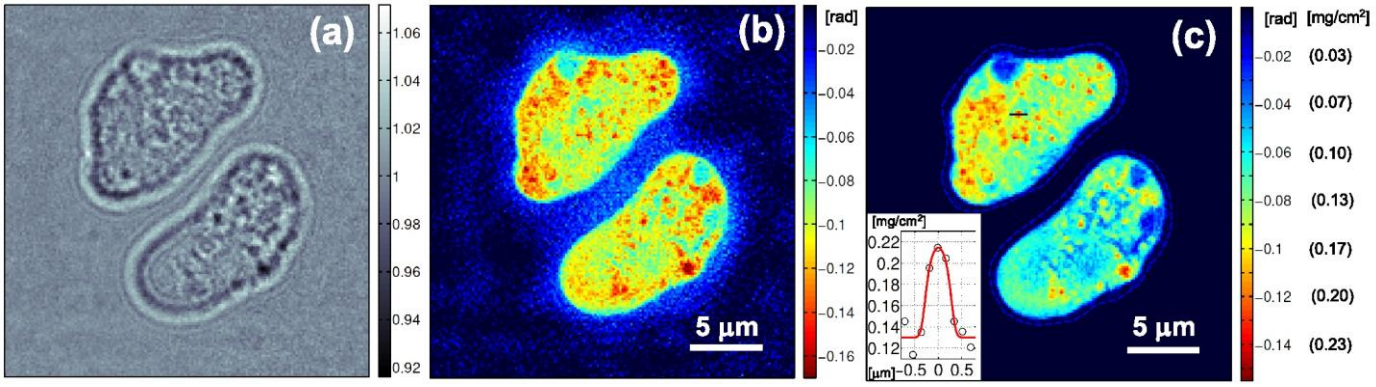

***Figure 24**: (a) Holographic intensity diffracted from freeze-dried D. discoideum cells, normalized by the empty WG intensity. (b) Iterative reconstruction of the object phase, obtained after 200 iterations of a Gerchberg-Saxton algorithm. (c) Phase reconstruction obtained with a modified HIO scheme for pure phase objects. The boundary of the support area was determined from a holographic reconstruction and is marked here by a dashed blue line. The colorbar is scaled in rad and also mg/cm^2, indicating the projected effective mass density of the cells. A line scan through a globular region of higher density is indicated in the upper cell by a thin black line and reproduced in the inset on the lower left. In addition to the reconstructed density, a model curve is given for the projected density of a spherical object with a diameter of 0.64 µm and an average volume density of 1.35 g/cm^3. To account for the finite spatial resolution the profile was convoluted by a normal distribution with a FWHM equal to the pixel size of 157 nm. Figure from [3].*

References

[1] Klaus Giewekemeyer, Pierre Thibault, Sebastian Kalbfleisch, André Beerlink, Cameron M. Kewish, Martin Dierolf, Franz Pfeiffer and Tim Salditt
Quantitative biological imaging by ptychographic x-ray diffraction microscopy
PNAS. 107 no. 2, 529-534 (2010)

[2] K. Giewekemeyer, H. Neubauer ,S. Kalbfleisch, S. P. Krüger and T. Salditt
Holographic and diffractive x-ray imaging using waveguides as quasi-point sources
New J. Phys. 12, 035008 (2010)

[3] K. Giewekemeyer, S.P. Krüger, S. Kalbfleisch, M. Bartels, C. Beta, and T. Salditt
X-ray propagation microscopy of biological cells using waveguides as a quasipoint source
Phys. Rev. A 83, 023804 (2011)

TU Dresden Group:

In preparation of the joint experiment at ESRF, the hard x-ray nanoprobe was optimized. In particular, a new generation of nanofocusing refractive x-ray lenses (NFLs) was fabricated. Keeping the nominal optical properties unchanged, the lens parameters were modified to avoid spherical aberrations. In the new design, the parabolic cylinder shape of the single lenses was changed from an elongated to a more round shape, thus avoiding shape anisotropies in the reactive ion etching process used to transfer the lens shape into the

silicon (cf. Fig. 25). In this way, the curvature of the individual lenses was enlarged, requiring an increased number of single lenses in one NFL.

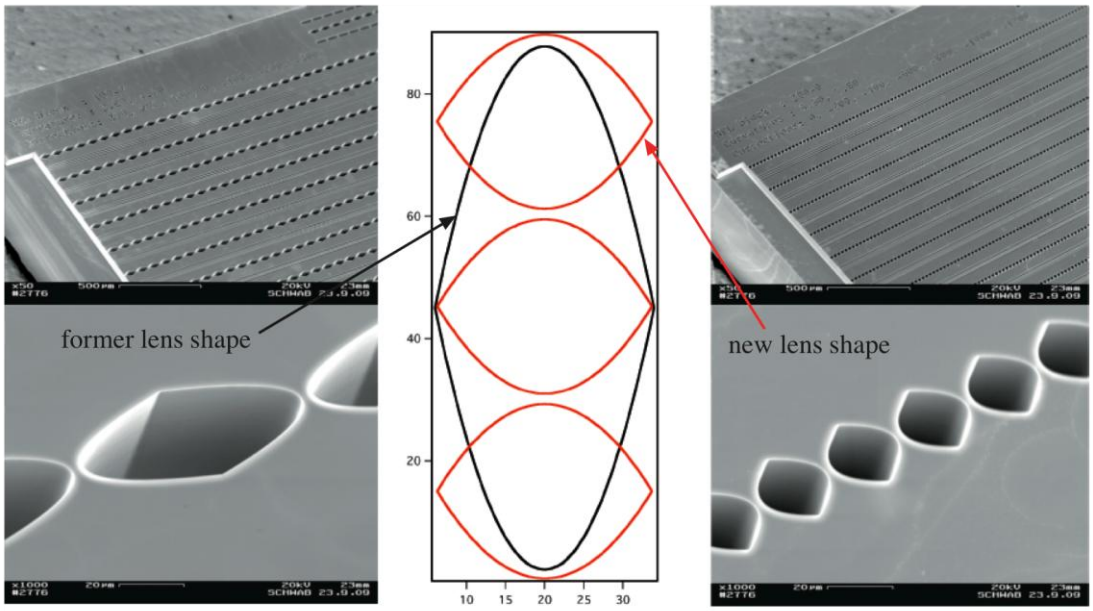

***Figure 25**: (left) previous, elongated lens shape: shape anisotropy during the etching process leads to spherical aberrations. (right) new, more round lens shape: underetching effects are more regular and can be compensated more easily.*

These new optics were fully characterized in our joint ESRF experiment in July 2009 using ptychography of a NTT-AT test pattern [1]. The method combines coherent x-ray diffraction with scanning microscopy. In this experiment the sample was scanned through the focus of the x-ray beam, and at each position a coherent far-field diffraction pattern was recorded. If the overlap between neighboring illuminated areas is sufficiently large the overdetermination allows one to reconstruct both the complex transmission function of the object as well as the complex incoming wave field. In Fig. 26 a) and Fig. 26 b) the reconstructed complex wave field in the focal plane is shown. It completely characterizes the wave field created by the refractive optics with both high spatial resolution and dynamic range in intensity. Just by numerically propagating this wave field along the beam direction the full caustic of the focused x-ray beam can be determined, cf. Fig. 26 c) [1]. The nearly Gaussian focus with a FWHM lateral extension of 78 x 86 nm^2 is close to ideal, showing that the new lens design is nearly free of spherical aberrations.

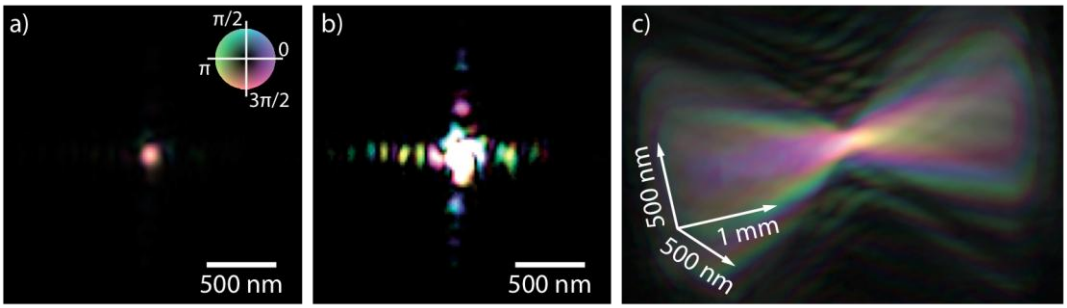

***Figure 26:** a) Reconstructed wave field in the nanofocus. Phase is expressed by the colorcode as given in the inset, amplitude by the brightness. b) The amplitude of the wave field is scaled such as to highlight low intensity side maxima. c) 3D view of the focused x-ray beam.*

The question of resolution limits in coherent x-ray diffraction imaging (CXDI) was investigated in a publication by A. Schropp and C. G. Schroer [2]. As the diffracted intensity is typically low for small samples and is characterized by a strong fall-off in intensity towards larger scattering angles, the achievable resolution is limited for radiation-hard samples by the incident photon density. We addressed the question of what dose is required to image an object by CXDI and to resolve a certain sub-unit or feature of that object. We show that a necessary condition for being able to resolve the detail is that the feature could be imaged by CXDI by itself. This allows one to easily estimate the dose requirements for identifying atoms and clusters in larger objects. Since the maximum number of photons per x-ray pulse is limited at free-electron laser sources the results will provide a significant contribution in the planning of future CXDI-experiments at these new sources.

By now, ptychographic imaging is performed routinely, both at the ESRF in Grenoble and at PETRA III. It is used to characterize the hard x-ray nanobeams and to enhance contrast and resolution in scanning microscopy. In early 2010, we applied this method to image quantitatively a front-end processed passivated microchip fabricated in 80 nm technology. The experiment was carried out at beamline ID13 of the ESRF at the nanoprobe station with nanofocusing refractive x-ray lenses. No sample preparation was needed to image buried interconnects and contact layers with a spatial resolution of slightly better than 40 nm. The ptychographic scanning coherent x-ray diffraction micrograph is shown in Fig. 27 (left). For comparison, the transmission, darkfield, and tungsten fluorescence signals are shown in Fig. 27 (right) that were recorded during the ptychographic scan. While transmission [Fig. 27a)] and darkfield [Fig. 27b)] particularly suffer from weak signal-to-noise ratio, the tungsten fluorescence [Fig. 27c)] shows good contrast due to the low background of x-ray fluorescence excited with monochromatic radiation. The best signal-to-noise ratio and a significantly increased spatial resolution is obtained in the ptychogram [Fig. 27d)]. Details are published in [3].

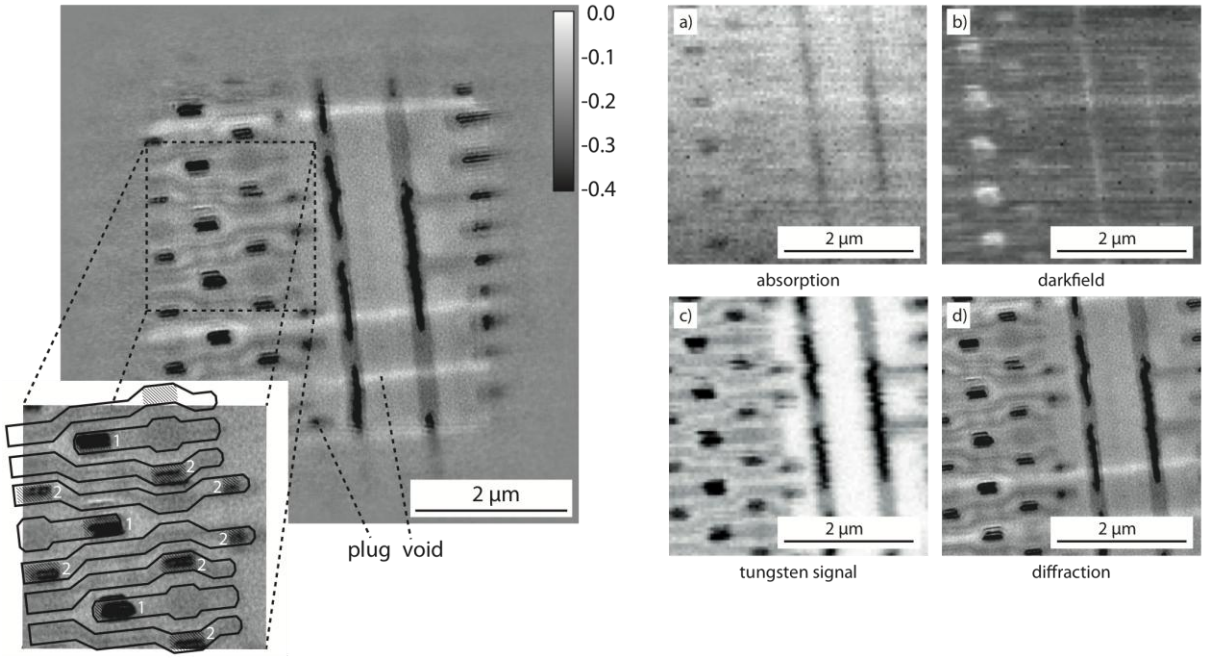

Figure 27: *Left: Ptychographic scanning diffraction micrograph of a front-end processed passivated microchip. Conductive paths are clearly resolved and are schematically redrawn in the inset for the dashed area. Right: a) transmission, b) darkfield, c) tungsten fluorescence contrast obtained during the ptychographic scan. In comparision, the ptychographic reconstruction is shown in d).*

References
[1] A. Schropp, et al., Appl. Phys. Lett. **96** (9), 091102 (2010).
[2] A. Schropp, C. G. Schroer, New Journal of Physics **12**, 035016 (2010).
[3] A. Schropp, et. al., J. Microscopy **241**, 9 (2011)

DESY group: Short Overview of the activities in 2010.

A.P. Mancuso, Th. Gorniak, F. Staier, O.M. Yefanov, R. Barth, C. Christophis, B. Reime, J. Gulden, A. Singer, M.E. Pettit, Th. Nisius, Th. Wilhein, C. Gutt, G. Grübel, N. Guerassimova, R. Treusch, J. Feldhaus, S. Eisebitt, E. Weckert, M. Grunze, A. Rosenhahn, and I. A. Vartanyants "Coherent imaging of biological samples with femtosecond pulses at the free-electron laser FLASH", Focus issue: Focus on X-ray beams with high coherence. New J. Phys. **12** 035003 (2010).

Coherent x-ray imaging represents a new window to imaging noncrystalline, biological specimens at unprecedented resolutions. The advent of free-electron lasers (FEL) allows extremely high flux densities to be delivered to a specimen resulting in stronger scattered signal from these samples to be measured. In the best case scenario, the diffraction pattern is measured *before* the sample is destroyed by these intense pulses, as the processes involved in radiation damage may be substantially slower than the pulse duration. In this case, the scattered signal can be interpreted and reconstructed to yield a faithful image of the sample at a resolution beyond the conventional radiation damage limit. We employ coherent x-ray diffraction imaging (CXDI) using the free-electron LASer in Hamburg (FLASH) in a *non-destructive* regime to compare images of a biological sample reconstructed using different, single, femtosecond pulses of FEL radiation. Furthermore, for the first time, we demonstrate CXDI, in-line holography and Fourier transform holography (FTH) of the same unicellular marine organism using an FEL and present diffraction data collected using the third harmonic of FLASH, reaching into the water window. We provide quantitative results for the resolution of the CXDI images as a function of pulse intensity, and compare this with the resolutions achieved with in-line holography and FTH.

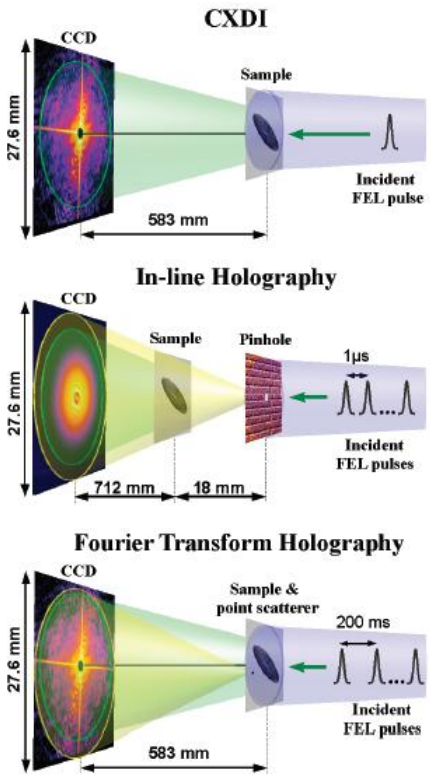

Figure 28:. *Schematic view of the different imaging experiments using coherent beams. (Top panel) CXDI experiment: a single pulse from the FEL first interacts with the sample, and then the diffracted radiation propagates to a CCD detector. (Middle panel) In-line holography experiment: single pulses from the FEL first scatter on the pinhole, then part of the reference beam interacts with the sample, and then the interference pattern is measured on a CCD detector. (Bottom panel) FTH experiment: single pulses from the FEL interact with the sample and reference point scatterer resulting in an interference pattern measured on a CCD detector.*

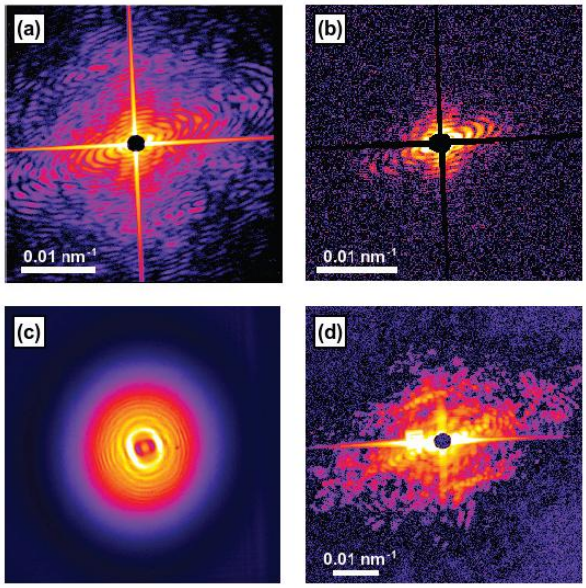

Figure 29: *Results of the coherent imaging experiment. (a) CXDI experiment. The sum of ten accumulated (30 s each) diffraction patterns measured at fundamental 8 nm wavelength. (b) The same as (a) for a single FEL pulse measurement with streaks and beamstop removed. (c) In-line holography diffraction pattern accumulated for 8 s. (d) Diffraction pattern measured at the third harmonic of the fundamental wavelength (2.66 nm) accumulated for 300 s. A nonlinear color scale is used to display these data. Logarithmic scale is used in (a, b, d).*

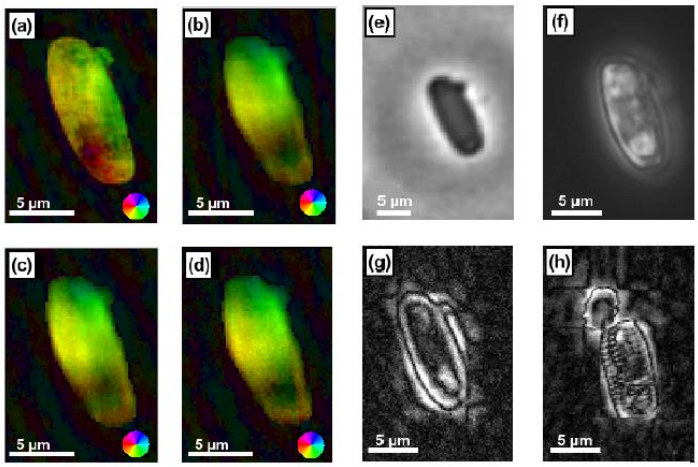

Figure 30: *(a)–(d) Reconstruction from the CXDI data. (a) Reconstructed image of a cell of N. perminuta from the integrated diffraction pattern (figure 2(a)). (b)–(d) Same from the different single-pulse diffraction patterns. (e) In-line holography reconstruction from the diatom cell. (f) Optical micrograph of the Navicula cell (20×, NA 0.45). (g) Reconstructed Fourier transform hologram of the diatom sample. (h) FTH reconstruction of a different N. perminuta cell. In (a)–(d), a color scale with the magnitude encoded in the value and the phase encoded in the hue of the image is implemented. The phase colormap is given by the wheel in the bottom right corner of the images.*

J. Gulden, O.M. Yefanov, A.P. Mancuso, V.V. Abramova, J. Hilhorst, D. Byelov, I. Snigireva, A. Snigirev, A.V. Petukhov, and I.A. Vartanyants " Coherent x-ray imaging of defects in colloidal crystals", Phys. Rev. B Vol. **81**, No. 22, 224105 (2010).

Coherent x-ray diffractive imaging (CXDI) was applied to reveal the structure of colloidal crystals. The colloidal sample was illuminated by a coherent x-ray beam through a 7 m pinhole aperture. The resulting diffraction patterns contain several Bragg peaks and an additional interference structure between the peaks due to the coherent illumination of a finite part of the sample. The inversion of these diffraction patterns reveals the arrangement of colloidal particles in a face-centered cubic (fcc) lattice as well as defects in the form of stacking faults in the (111) planes.

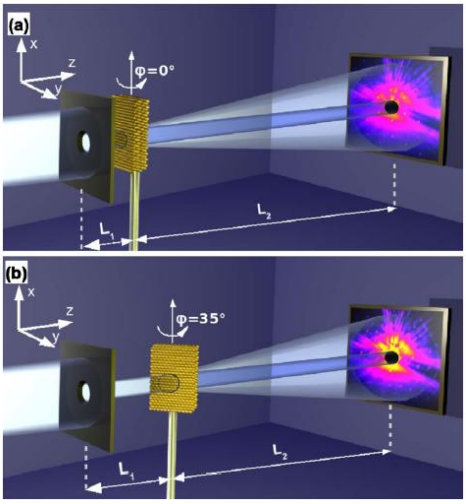

Figure 31*:Schematic view of the CXDI experiment showing the pinhole, the sample and the detector. (a) Measurements at azimuthal angle φ=0° (b) φ =35°.*

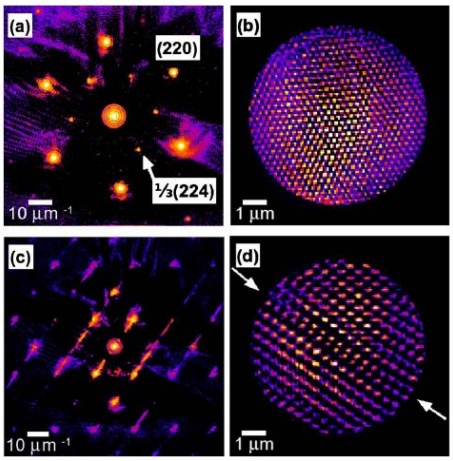

Figure 32: *[(a) and (c)] Difference diffraction patterns (in logarithmic scale) obtained as a result of the subtraction of the scaled diffraction pattern of the pinhole from the measured diffraction patterns of the sample (a) φ =0, (c) φ =35°. Black regions correspond to negative values and were left to evolve freely in the reconstruction. The central part around q=0 was implemented from the result of the reconstruction after 20 iterations.[(b) and (d)] Reconstruction of the colloidal sample from the diffraction patterns (a) φ =0, (c) φ =35°. The arrows in (d) point to the defect in the crystal.*